Quaternary Science Reviews 195 (2018) 32–47

Contents lists available at ScienceDirect

Quaternary Science Reviews

journal homepage: www.elsevier.com/locate/quascirev

Atmosphere-driven ice sheet mass loss paced by topography: Insights from modelling the south-western Scandinavian Ice Sheet

Henning Åkesson [a, *], Mathieu Morlighem [b], Kerim H. Nisancioglu [a, c], John Inge Svendsen [a], Jan Mangerud [a]

[a] Department of Earth Science, University of Bergen and Bjerknes Centre for Climate Research, Allégaten 70, 5007, Bergen, Norway
[b] University of California, Irvine, Department of Earth System Science, 3218 Croul Hall, Irvine, CA, 92697-3100, USA
[c] Centre for Earth Evolution and Dynamics, University of Oslo, Postbox 1028 Blindern, 0315, Oslo, Norway

ARTICLE INFO

Article history:
Received 20 December 2017
Received in revised form
16 April 2018
Accepted 4 July 2018
Available online 17 July 2018

Keywords:
Ice sheet modelling
Grounding line dynamics
Marine-terminating glaciers
Deglaciation
Ice-ocean interactions
Surface mass balance
Younger dryas
Norway
Eurasian ice sheet
Scandinavian ice sheet

ABSTRACT

Marine-terminating glaciers and ice streams are important controls of ice sheet mass balance. However, understanding of their long-term response to external forcing is limited by relatively short observational records of present-day glaciers and sparse geologic evidence for paleo-glaciers. Here we use a high-resolution ice sheet model with an accurate representation of grounding line dynamics to study the deglaciation of the marine-based south-western Norwegian sector of the Scandinavian Ice Sheet and its sensitivity to ocean and atmosphere forcing. We find that the regional response to a uniform climate change is highly dependent on the local bedrock topography, consistent with ice sheet reconstructions. Our simulations suggest that ocean warming is able to trigger initial retreat in several fjords, but is not sufficient to explain retreat everywhere. Widespread retreat requires additional ice thinning driven by surface melt. Once retreat is triggered, the underlying bedrock topography and fjord width control the rate and extent of retreat, while multi-millennial changes over the course of deglaciation are modulated by surface melt. We suggest that fjord geometry, ice-ocean interactions and grounding line dynamics are vital controls of decadal-to centennial scale ice sheet mass loss. However, we postulate that atmospheric changes are the most important drivers of widespread ice sheet demise, and will likely trump oceanic influence on future ice sheet mass loss and resulting sea level rise over centennial and longer time scales.

1. Introduction

Ice streams and marine-terminating glaciers are capable of rapidly discharging significant amounts of ice into the ocean. Their response to the current climate warming trend remains a major uncertainty in projections of future ice sheet mass loss and sea level rise (Nick et al., 2013; Nowicki et al., 2013; Ritz et al., 2015). Outlet glaciers and ice shelves in Greenland and Antarctica are retreating (e.g. Moon and Joughin, 2008; Murray et al., 2015), accelerating (Moon et al., 2012; Joughin et al., 2014), thinning (Pritchard et al., 2009; Paolo et al., 2015), and weakening (Borstad et al., 2013; Fürst et al., 2016). The bed topography of most major outlet glaciers remains below sea level far inland (Morlighem et al., 2014; Fretwell et al., 2013; An et al., 2017; Millan et al., 2017), making present day glaciers vulnerable to warm ocean waters as grounding lines retreat. Moreover, some beds deepen inland, a configuration associated with a potential marine ice sheet instability (e.g. Weertman, 1974; Feldmann and Levermann, 2015; Golledge et al., 2015). The latter conditions suggest that dynamic mass loss, once triggered, may continue largely decoupled from future changes to external forcing and associated efforts to decrease anthropogenic emissions. For marine margins buttressed by ice shelves, or for glaciers terminating in fjords, it is uncertain to what extent such accelerated mass loss will take place, given the additional support provided by ice shelves and trough walls (Schoof et al., 2017; Haseloff and Sergienko, 2018; Åkesson et al., 2018).

It is unclear for how long accelerated ice discharge can be sustained, and it is therefore crucial to assess the relative importance of the drivers of mass loss over centennial-to millennial-scales. A leading hypothesis explaining contemporary changes to marine terminating glaciers and ice shelves is the intrusion of warm subsurface waters reaching ice shelf drafts and glacier grounding lines (Holland et al., 2008; Straneo and Heimbach, 2013). However,

* Corresponding author.
E-mail address: henning.akesson@geo.su.se (H. Åkesson).

https://doi.org/10.1016/j.quascirev.2018.07.004

reconstructions and model studies are inconclusive with regards to whether high surface melt or ocean-driven dynamic mass loss control long term ice sheet stability and sea level rise (Golledge et al., 2015; Stokes et al., 2016).

Another source of uncertainty is which glaciers are most vulnerable, and whether their responses are non-linear (Reyes et al., 2014; Dutton et al., 2015; Mengel and Levermann, 2014; Mengel et al., 2016). Both empirical ice sheet reconstructions (Mangerud et al., 2013, 2016; Stokes et al., 2014) and modern observations (Moon et al., 2012; Bartholomaus et al., 2016; Felikson et al., 2017) show that responses vary even within regions experiencing similar external forcings. This behaviour, apparently out-of-phase with contemporary climate, complicates interpretation of observations and excludes marine-terminating glaciers as past climate indicators without additional knowledge of site-specific controls.

Our ability to model past ice sheet change provides an important metric to evaluate the accuracy of numerical models used for future predictions. To test the accuracy of these models, geologic evidence can be used. However, sedimentary and geomorphologic data provide only mean rates of change, constrained by dating accuracy. Short-term variations may thus be masked out and interpretations hampered. For example, glacier moraines may be deposited several hundreds or thousand years apart. Cosmogenically dated erratics, though useful to map ice-free surfaces, have uncertainties in the centennial to millennial range (e.g. Briner et al., 2005). These types of evidence provide only snapshots in time. Sedimentary sequences, in contrast, are inherently continuous. Yet, their spatial coverage is sparse; to elucidate whether they represent a regional ice sheet margin or a local anomalous feature requires many samples and extensive field studies.

While certainly having limitations, numerical ice sheet models give a continuous and spatially complete picture, and can resolve ephemeral behaviour. Models can also help disentangle the extent to which external forcing or site-specific factors dominate glacier behaviour. Numerous large-scale, transient simulations of the deglaciation of past ice sheets have been carried out. Studies of the Antarctic (Golledge et al., 2012; Pollard et al., 2015), Greenland (Robinson et al., 2011; Applegate et al., 2012), British-Irish (Hubbard et al., 2009), Laurentide (Marshall et al., 2000; Tarasov et al., 2012), and Eurasian Ice Sheets (Arnold and Sharp, 2002; Kleman et al., 2002; Patton et al., 2017) have all improved our understanding of long-term ice sheet change. However, marine-terminating glaciers, distributed all around the coasts of Greenland, Norway, Svalbard, Patagonia, Alaska, and parts of Antarctica, are often too small to be resolved accurately in such coarsely resolved large-scale ice sheet models. This issue limits model accuracy and our understanding of past behaviour. Many paleo-ice sheet models rely solely on the computationally-efficient Shallow Ice Approximation (Hutter, 1983; Morland, 1984), which is unable to capture interactions between fast-flowing ice streams and the interior ice sheet.

One of the most important physical processes that needs to be correctly captured by models is grounding line dynamics (e.g. Schoof, 2007), for which accurate representation requires spatial scales of ~1 km or better (Vieli and Payne, 2005; Durand et al., 2011; Seroussi et al., 2014; Gagliardini et al., 2016). Currently, computational constraints prevent continental-scale, high-resolution, transient paleo-simulations, i.e. several thousand years and longer at a resolution of ~1 km. Most work to date has therefore been on (i) coarse spatial and long temporal scales; or (ii) fine spatial and short temporal scales.

Flowline models remain an exception, as they can finely track grounding line motion over long time scales. These models have been used to study Antarctic ice streams (Jamieson et al., 2012, 2014), Greenlandic outlet glaciers (Nick et al., 2009, 2013; Vieli and Nick, 2011; Lea et al., 2014; Steiger et al., 2018), as well as idealised glaciers (e.g. Vieli et al., 2001; Nick et al., 2010; Enderlin et al., 2013; Åkesson et al., 2018). While useful to better understand physical processes, including calving dynamics, flowline models are not suitable for complex geometries, nor can they capture interactions between neighbouring drainage basins. These models are also width-averaged by definition, which precludes accurate representation of across-flow topographic features such as local pinning points.

Here, we use an alternative approach to simulate the deglaciation of south-western Norway by applying a high resolution, regional ice sheet model to assess this area's sensitivity to ocean and atmospheric warming. We resolve individual fjords and their interactions, and provide a spatially complete, transient picture from 18 to 11 ka before present (BP). South-western Norway was the marine-based western Norwegian sector of the Scandinavian Ice Sheet and is exceptionally data-rich (e.g. Hughes et al., 2016; Mangerud et al., 2017), yet the ice sheet behaviour has not been studied in a detailed model framework before.

This paper is structured as follows. First, we briefly describe relevant ice sheet changes in south-western Norway over the modelled period 18–11 ka BP (Sect. 2). Details of the ice sheet model and implementation of atmosphere and ocean forcing are given in Sect. 3, followed by a description of experimental design and empirical constraints (Sect. 4). Our results are divided into sensitivity experiments to forcing from the ocean (Sect. 5.2) and the atmosphere (Sect. 5.3), as well as simulations of the deglaciation 18–11 ka BP (Sect. 5.4). We discuss the relative influence of the forcing (Sect. 6.1), topography (Sect. 6.2), as well as model limitations (Sect. 6.3), and finally highlight implications for past and future stability of ice sheets in Sect. 6.4.

2. Deglacial history of south-western Norway

During the Last Glacial Maximum (LGM) c. 21–20 ka BP, the Scandinavian Ice Sheet was connected with the British-Irish Ice Sheet (e.g. Hughes et al., 2016). Subsequently, the major Norwegian Channel Ice Stream was activated in the Norwegian Channel. This ice stream flowed northwards along the west coast of Norway before collapsing 19–18 ka BP (Svendsen et al., 2015; Sejrup et al., 2016). Here we do not model these early phases, instead we examine the triggers and drivers of deglaciation of south-western Norway over the period 18–11 ka BP. Once the Norwegian Channel Ice Stream collapsed, a new stable ice margin roughly parallel with the Norwegian coast was established (Mangerud et al., 2017) (see Fig. 1). Our simulations start from this period, when western Norway resembled present-day Greenland, with marine-terminating glaciers and deeply incised subglacial valleys draining the interior ice sheet (Morlighem et al., 2014, 2017).

Deglaciation of western Norway started around 18 ka BP with the southernmost offshore islands and coastal areas becoming ice-free first (Fig. 2). In contrast, coastal areas farther north remained ice-covered until 15 ka BP, during which time sea surface temperatures (SSTs) remained relatively stable in the Norwegian Sea (Eldevik et al., 2014; Dokken et al., 2015). Widespread retreat in western Norway only occurred after 15 ka BP. The paleoclimate record suggests an asynchronous retreat history across different outlet glaciers, despite similar changes to the maritime climate. Stratigraphic evidence from lakes and bogs, as well as cosmogenically dated erratics, suggest that retreat of the Boknafjorden outlet glacier and Jæren regions (Fig. 2) to the south commenced 17–16 ka (Briner et al., 2014; Svendsen et al., 2015; Lunnan, 2016; Johnsen, 2017; Gump et al., 2017). In contrast, Hardangerfjorden glacier,

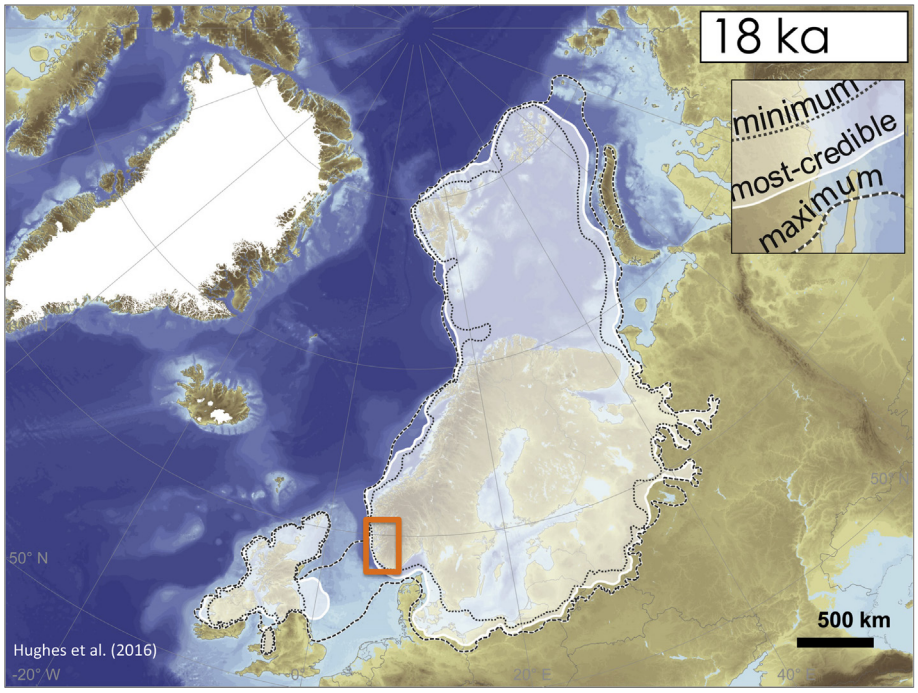

Fig. 1. Reconstructed Eurasian Ice Sheet extent (Hughes et al., 2016) for our initial model state at 18 ka BP. Ice sheet retreat is simulated within the indicated orange area. (For interpretation of the references to colour in this figure legend, the reader is referred to the Web version of this article.)

only 50 km north, started to retreat 1–2000 years later, at the transition into the warm Bølling inderstadial c. 14.8 ka BP (Mangerud et al., 2013, 2016).

During the Bølling-Allerød c. 14.8–12.7 ka BP, ice sheet retreat was extensive (Fig. 2), with margins in some areas retreating c. 40–50 km inland of their subsequent Younger Dryas (YD) positions. Readvance during the following YD cold reversal c. 12.7–11.6 ka BP produced prominent moraines that can be traced from sea level to the high uplands (Andersen, 1954; Follestad, 1972). This YD readvance overran any Allerød deposits, erasing evidence of the ice configuration prior to the YD, for which knowledge is limited to stratigraphic records (Mangerud et al., 2016).

Reconstructions thus imply that retreat during deglaciation in western Norway differed between outlet glaciers (Mangerud et al., 2013, 2016; Briner et al., 2014; Gump et al., 2017). Similarly, Stokes et al. (2014) suggested that retreat of marine-terminating glaciers in northern Norway during deglaciation 15–10 ka BP was out-of-phase with contemporary climate changes. These lines of evidence suggest that glacier-specific factors such as local topography alter the expected response to the climate forcing. Nevertheless, quantitative explanations of these intraregional differences are yet to be established.

3. Ice sheet model

3.1. Ice dynamics and model mesh

We use the two-dimensional Shelfy Stream Approximation (SSA, MacAyeal, 1989) within the Ice Sheet System Model (ISSM, Larour et al., 2012). This stress balance approximation is well suited to model fast ice streams and regions experiencing significant sliding at the bed. In contrast to the Shallow Ice Approximation (Hutter, 1983; Morland, 1984), commonly used in paleoclimate studies, the SSA includes a non-local stress balance, accounting for membrane stresses. The SSA also significantly reduces the computational cost compared to higher-order ice flow physics. Note, however, that SSA is less suited for land-based flow, where internal deformation is important.

We construct a non-uniform model mesh with resolution varying from 1 km in areas of high basal relief, to 10 km in areas with smoother topography. In addition, we enforce 1 km resolution in all areas below sea level, consistent with requirements to accurately simulate grounding line dynamics (Durand et al., 2011; Seroussi et al., 2014). In practice, a resolution of 1 km is enough to accurately capture grounding line dynamics when using a subelement hydrostatic scheme (Seroussi et al., 2014) developed for this purpose.

Ice is assumed isothermal with a viscosity equivalent to an ice temperature of -5°C (Cuffey and Paterson, 2010, p.73; rate factor listed in Table 1), consistent with what is used in model studies for the western and eastern Greenland Ice Sheet (e.g. Nick et al., 2013).

Our model domain is restricted to south-western Norway, and we assume a fixed ice divide corresponding to present-day water divides (Fig. 2) with no influx into our domain. In contrast to our model, the ice divide likely migrated over the course of deglaciation. However, we make this assumption for simplicity and technical reasons, avoiding unphysical model behaviour associated with an imposed migration of the ice divide. We assess this approach by comparing with large-scale model output of the Eurasian Ice Sheet (L. Tarasov, unpubl. data). This assumption is reasonable for the later part of the deglaciation, and less accurate for the earlier part, when the ice divide is likely to have been located further east. However, since this is far from the ice sheet margin in the early part of our deglaciation simulation (18–15 ka), and modelled ice flow in the interior is slow, we find this bias acceptable.

While we accurately model grounding line migration, we deliberately neglect migration of the floating ice front as we do not have sufficient data to calibrate a calving model. Note, however, that the floating tongue is affected by oceanic melt and will impact the stability of the glacier.

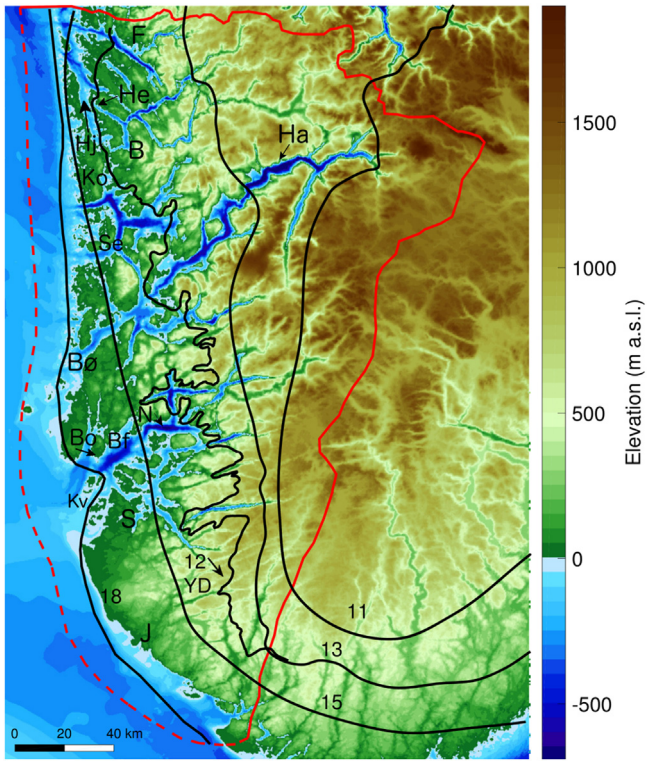

Fig. 2. Map of southwestern Norway showing the model domain following present-day water divides (red solid line), western model boundary (red dashed line), approximate reconstructed ice margins for 18 ka (Hughes et al., 2016; Gump et al., 2017), 15 ka, 13 ka, 11 ka, and the well-constrained reconstructed margin at the Younger Dryas (YD) maximum c. 12 ka (Ehlers et al., 2011; Mangerud et al., 2013, 2017; Briner et al., 2014; Hughes et al., 2016; Gump et al., 2017). Place names from north to south: F–Fensfjorden, He–Herdla, Hj–Hjeltefjorden, Ha–Hardangerfjorden, B–Bergen, Ko–Korsfjorden, Se–Selbjørnsfjorden, Bø–Bømlafjorden, N–Nedstrandsfjorden, Bo–Bokn, Bf–Boknafjorden, Kv-Kvitsøy, S-Stavanger, J–Jæren. (For interpretation of the references to colour in this figure legend, the reader is referred to the Web version of this article.)

3.2. Basal conditions for grounded ice

Basal motion is modelled using a linearly viscous sliding law (Budd et al., 1984):

$$\tau_b = -\alpha^2 N_e v_b, \tag{1}$$

where τ_b is the basal drag, α is a friction parameter, v_b is the basal velocity and N_e the effective pressure. We assume that the subglacial hydrological system is a uniform sheet of water connected to the ocean, and the effective pressure is taken as the difference between the weight of ice and the hydrostatic height: $N_e = \rho_i g H - \rho_w g |z_b|$, where ρ_i, g, H, ρ_w, and z_b are ice density, gravitational acceleration, ice thickness, freshwater density and bed elevation, respectively. We construct a spatially variable basal drag coefficient α proportional to bed elevation z_b:

$$\alpha = 120 \frac{\min(\max(0, z_b + 800), 2000)}{2000} \tag{2}$$

Using this simple approach, we capture the expected fast flow (low drag) in the fjords, and simulate slow flow (high drag) on uplands and in the ice sheet interior. No friction ($\alpha = 0$) is applied for floating ice. In some areas in the interior, thin-ice areas might have been frozen to the bed (e.g. Kleman and Hättestrand, 1999). This is implicitly accounted for by introducing a very high basal drag at high elevations, where we expect ice to be thin.

3.3. Surface mass balance

For simplicity, we represent changes in surface mass balance by imposing variations in the equilibrium line altitude (ELA). The strength of this approach is that the ELA implicitly accounts for changes in summer and winter surface mass balance, for which knowledge of a number of near-surface processes is not available. We thereby avoid tuning a suite of poorly constrained parameters required for a surface energy balance (Hock, 2005) or insolation-temperature model (e.g. Robinson et al., 2010). An alternative would have been to use a simple positive-degree day (PDD) model (e.g. Reeh, 1989; Hock, 2003). However, they require calibration of melt factors for snow and ice, which are not known for this region in the past.

Temperature and precipitation records are also poorly constrained during deglaciation. This is especially true for the first few thousand years, when most of south-westernern Norway was ice-covered, preventing formation of terrestrial records.

Observed ELAs in western Norway follow an E-W gradient gradually falling towards the coast (Østrem and Liestøl, 1964). We define a spatially variable initial reference $\mathrm{ELA}(x,y)_{ref}$ based on present-day ELAs (Lie et al., 2003a; b; Andreassen et al., 2005; Giesen and Oerlemans, 2010). The ice surface is oriented approximately parallel to this E-W gradient. We therefore represent the gradient by constructing an $\mathrm{ELA}(x,y)_{ref}$ as a function of the initial (pre-spinup) surface elevation z_s (see Sect. 4.1):

$$ELA(x,y)_{ref} = 300 + 0.42 z_s. \tag{3}$$

This function is a simplification of the detailed spatial maps of ELA for southern Norway calculated by Lie et al. (2003b). The latter

Table 1
Constants and parameter values used in this study.

Parameter	Symbol	Value	Unit
Ice density	ρ_i	917	kg m^{-3}
Freshwater density	ρ_w	1000	kg m^{-3}
Gravitational acceleration	g	9.81	m s^{-2}
Rate factor	A	1.0753×10^{-24}	s^{-1} Pa^{-3}
Basal friction parameter	α	0–120	(Pa a^{-1})$^{1/2}$
Sliding law exponent	m	1	
Glen's law exponent	n	3	
Vertical SMB gradient, ablation zone	Γ_{abl}	0.0037	a^{-1}
Vertical SMB gradient, accumulation zone	Γ_{acc}	0.002	a^{-1}
Upper bound on SMB	$\dot{B}_{max}$	1	m w.e.
Lower bound on SMB	$\dot{B}_{min}$	−6	m w.e.
Mesh resolution	Δx	1–15	km
Time step	Δt	0.05	a

calculated ELAs based on modern temperature and precipitation records for southern Norway, using observed ELAs from local glaciers and ice caps as validation.

A temporally varying ELA is calculated by adding an time-dependent anomaly $\Delta ELA(t)$ to the initial reference $\mathrm{ELA}(x,y)_{ref}$:

$$ELA(x,y,t) = ELA(x,y)_{ref} + \Delta ELA(t). \quad (4)$$

We thus have a spatially varying surface forcing, with temporal changes applied uniformly in space. Here, the temporal changes ($\Delta ELA(t)$) will be based on reconstructions for the deglaciation (see Sect. 4.3).

An elevation dependent surface mass balance rate $\dot{B}$ is calculated using separate vertical mass balance gradients Γ_{abl} and Γ_{acc} in the ablation and accumulation zones, respectively (see Table 1). These gradients are based on present-day and past studies of Greenland, Alaska, and Norway (Van de Wal, 1996; Van de Wal et al., 2005; Rea and Evans, 2007; Van Beusekom et al., 2010; Huss and Farinotti, 2012), which is representative of the regional climate in our modelled area. We also compared our gradients against large-scale, coarse-resolution simulations of the entire Eurasian Ice Sheet (L. Tarasov, unpubl. data) and found our gradients to be appropriate time-averaged values for the deglaciation.

In the ablation zone, $\dot{B}$ at a certain elevation z is calculated by

$$\dot{B}(z) = \max\left(\Gamma_{abl}(z - ELA(x,y,t)), \dot{B}_{min}\right), \quad (5)$$

and similarly, in the accumulation zone

$$\dot{B}(z) = \min\left(\Gamma_{acc}(z - ELA(x,y,t)), \dot{B}_{max}\right), \quad (6)$$

The limits of $\dot{B}_{min} = -6$ m water equivalent (w.e.) and $\dot{B}_{max} = 1$ m w. e. are introduced to avoid unphysical surface mass balance rates and are consistent with a range of observations from the Greenland Ice Sheet and Alaska (Van de Wal, 1996; Van de Wal et al., 2005; Van Beusekom et al., 2010; Helsen et al., 2012).

3.4. Ocean forcing

At the base of ice shelves, we apply a uniform reference submarine melt rate $\dot{M}_{ref} = 20\ \mathrm{m\ a^{-1}}$. This melt rate is close to observations of Greenland outlet glaciers (Rignot et al., 2010) and Antarctic ice shelves (Rignot et al., 2013). We expect ocean conditions for the Norwegian coast to be similar, considering changes in sea surface temperatures (SSTs) reconstructed for the Norwegian Sea during deglaciation (Bakke et al., 2009; Eldevik et al., 2014; Dokken et al., 2015). For simulations of the deglaciation, submarine melt rates are scaled with atmospheric forcing as follows:

$$\dot{M} = \dot{M}_{ref} + 0.05a^{-1}\Delta ELA(t), \quad (7)$$

where $\Delta ELA(t)$ is given in Fig. 9a (see details in Sect. 4.3). This corresponds to a 1:20 submarine melt rate to ELA scaling, e.g., a 100 m change in ELA implies a 5 m $\mathrm{a^{-1}}$ change in submarine melt rate. This scaling assumes that atmosphere and ocean changes are coupled on the centennial to millennial time-scales considered here. This coupling may occur via direct air-sea interactions, or through varying atmospheric-induced runoff, resulting in subglacial discharge and changes in submarine melt (Slater et al., 2016). Melt rate magnitudes are arbitrary yet consistent with measured submarine melt rates on Greenland (Rignot et al., 2010; Motyka et al., 2011; Fried et al., 2015).

4. Experimental design and empirical constraints

4.1. Initial conditions

As initial conditions we impose a simplified representation of the 18 ka ice sheet. We choose 18 ka as a starting point since the Norwegian Channel Ice Stream collapsed prior to this time (Svendsen et al., 2015; Sejrup et al., 2016; Morén et al., 2017). This means the ice sheet margin was at the coast, similar, albeit slightly more extensive than the margins of the Greenland Ice Sheet today. We initialise our ice sheet model with estimated 18 ka grounding lines based on empirical evidence (Hughes et al., 2016; Gump et al., 2017; Mangerud et al., 2017). As the 18 ka grounding line positions are not well constrained, we let the grounding line evolve freely during a spin-up period, relaxing it to a stable position. We start with a polynomial-shaped ice sheet surface covering all sites of younger ^{10}Be exposure dates (Mangerud et al., 2013; Briner et al., 2014; Svendsen et al., 2015; Gump et al., 2017), and such that the interior ice sheet surface is in approximate agreement with Eurasian Ice Sheet simulations (L. Tarasov, unpubl. data). The spinup simulation is run for 2000 years using fixed model parameters and a constant climate with ELA_{ref}. We assume that the model reaches steady-state when rates of thickness change is smaller than 1 cm per year. Empirical evidence document a gradually falling relative sea level during deglaciation (Lohne et al., 2007; Lunnan, 2016). We therefore run our simulations using a sea level 20 m higher than today, in line with deglaciation-averaged sea levels from these reconstructions.

4.2. Sensitivity to atmospheric and ocean forcing

To quantify the ice sheet response to climate change, we perform a sensitivity study to step changes in surface mass balance

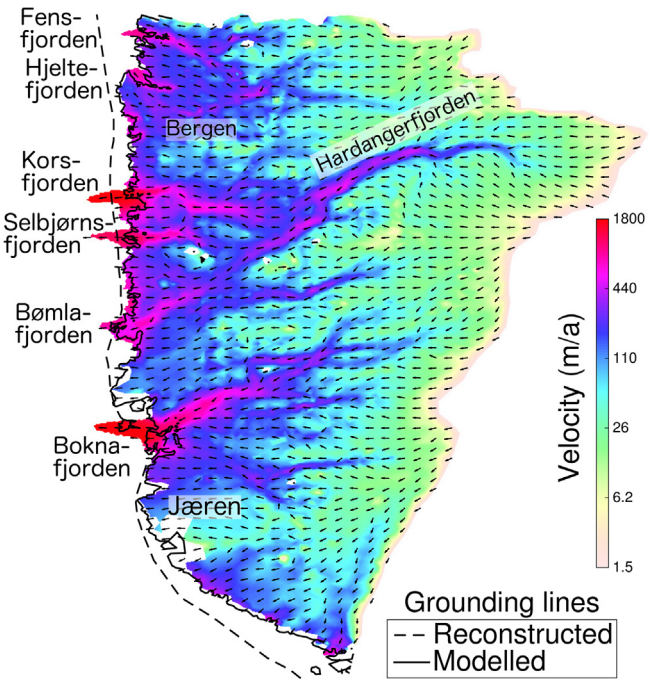

Fig. 3. High-resolution, steady-state velocity field at the end of the model spinup phase at 18 ka BP. The reconstructed grounding line is from 18 ka, also shown as '18' in Fig. 2. The velocity field is shown for areas with ice-cover within the model domain. See red-lined delineated area in Fig. 2 for map reference. Note log-scale. (For interpretation of the references to colour in this figure legend, the reader is referred to the Web version of this article.)

and submarine melt relative to the 18 ka model steady-state (Fig. 3).

Perturbations to the ELA range from +100 to +1200 m relative to 18 ka ELAs. For comparison, Younger Dryas ELAs are estimated to be c. 500 m higher than those at 18 ka, while present-day ELAs are c. 1000 m higher than 18 ka ELAs (Andreassen et al., 2005; Mangerud et al., 2016).

Submarine melt rates are perturbed in two separate sensitivity experiments, increasing from the reference melt rate $\dot{M}_{ref} = 20$ m a^{-1} at 18 ka, to 100 and 200 m a^{-1}.

Following these step perturbations of the ELA and submarine melt rates, starting with the 18 ka ice sheet, we let the model evolve to a new steady-state. In reality, changes would not have been instantaneous, or as large as applied here. The rationale behind making step changes, as opposed to a time-dependent forcing, is to isolate the relative ice sheet response to a different atmosphere and ocean, irrespective of the time scale of the forcing.

4.3. Deglaciation 18–11 ka

To model the deglaciation, we use the time-varying function $\Delta ELA(t)$, developed from a conceptual curve in Mangerud et al. (2016), as our atmosphere forcing (Fig. 9a). In order to scale this curve we have used the Younger Dryas ELA determined from the highest Younger Dryas lateral moraines, the present day ELA for the early Holocene (11 ka), and available paleoclimate reconstructions to estimate $\Delta ELA(t)$ for the rest of the period.

One of our objectives is to quantify the significance of ocean forcing as a driver of long-term ice sheet mass loss. To test this, we perform two parallel experiments for the period 18–11 ka using different submarine melt rates: (i) constant at 20 m a^{-1}, (ii) time-dependent, scaled to $\Delta ELA(t)$ over the course of deglaciation (Eq. (7); Fig. 9a).

Reconstructions of Norwegian Sea SSTs exist for the deglaciation (Bakke et al., 2009; Eldevik et al., 2014; Dokken et al., 2015). However, these do not give sufficient basis to spatially refine submarine melt rates in our region. We therefore keep our external forcing spatially uniform throughout the simulations.

5. Results

5.1. Ice sheet flow at 18 ka

For the state at 18 ka BP, we compare modelled ice velocities and flow directions (Fig. 3) with observations of glacial striae. In the entire area north of Korsfjorden and northwest of Hardangerfjorden (cf. Fig. 2) the model shows overall westward ice-flow across mountain areas. The ice flow direction is modulated by the underlying topography, particularly by the major fjords, where velocities are higher. However, note that the simulated ice-flow is unobstructed by several deep N–S trending fjords.

The simulated ice-flow across fjords is consistent with the oldest recorded glacial striae. These striae, found on the westernmost islands and on mountain summits inland, are all directed west towards the coast. These observations suggest that ice flow at the early stages of the deglaciation, when the ice was thick, was relatively independent of the underlying bed topography (Aarseth and Mangerud, 1974; Aa and Mangerud, 1981; Hamborg and Mangerud, 1981; Sæle, 2017). During the deglaciation, as the ice became thinner, the glacial striae show that the ice movement gradually became controlled by the bed topography.

The model shows westward ice flow out of the outer half of Hardangerfjorden, which is the longest and deepest fjord in the area, a picture consistent with glacial striae (Follestad, 1972; Holtedahl, 1975; Hamborg and Mangerud, 1981). Further south, the pattern of striae is more complicated, but for the western part, it is reasonably consistent with our modelled directions (Ringen, 1963; Rønnevik, 1971; Anundsen, 1972, 1990). We also note that there are locally conflicting ice movements between the model and observations, for which we have no straightforward explanation. For example, Andersen and Wangen (1987) found that ice flow was directed out of Boknafjorden and across northern Jæren, in contrast to our model results, which show ice-flow directions towards the Boknafjorden trough. Since modelled flow directions appear sensitive to underlying topography in coastal areas with thinner ice, a potential explanation is that an underestimated ice thickness leads to local flow inconsistent with the empirical evidence. Indeed, ^{10}Be exposure ages indicate that mountains which featured as small nunataks in the 18 ka model scenario were still covered by ice at this time, suggesting that the model underestimates ice thickness slightly in coastal areas.

5.2. Ocean forcing as a selective trigger

We start with a sensitivity study of the 18 ka ice sheet as described in Sect. 4.2. A spatially uniform increase in submarine melt rates from 20 to 100 m a^{-1} causes significant differences in timing and magnitude of grounding line retreat between fjords (Fig. 4). Retreat occurs through deep sections of the northernmost fjords in our domain (Fensfjorden and Hjeltefjorden), despite these fjords being relatively narrow (~ 3–5 km). A lack of prominent sills gives a ~25 km retreat in Fensfjorden, compared to 5–10 km in the nearby Hjeltefjorden, where the grounding line stabilises just south of the YD moraine at Herdla (e.g. Aarseth and Mangerud, 1974; Mangerud et al., 2016). Our sensitivity experiment is not meant to represent YD climate conditions, but the simulated stable grounding line off Herdla is consistent with reconstructions for the YD.

In stark contrast to the significant retreat in the north, the grounding line retreats only a few kilometres at the three narrow, shallow fjord mouths in the center of our domain (Korsfjorden, Selbjørnsfjorden, Bømlafjorden; Fig. 4). In the south, the most sensitive area is Boknafjorden. Fast-flowing ice in the main trough of Boknafjorden is fed by multiple tributaries from the east and south (Fig. 3). Following the increase in submarine melt (to 100 m a^{-1}), Boknafjorden's grounding line is dislodged from a ~200 m shallow sill south of the island Bokn and retreats ~25 km inland in less than 30 years, with a mean retreat rate exceeding 800 m a^{-1}. The grounding line stabilises a few kilometres upstream on a second sill (at km 55 in Fig. 5a). The glacier speeds up by 40% during the fast retreat, but slows down and flows only 5–10% faster at its new stable position compared to before retreat (Fig. 5b).

In our sensitivity experiments with a higher submarine melt rate of 200 m a^{-1} (Fig. 6), comparable to present-day Jakobshavn Isbræ in Greenland (Motyka et al., 2011), retreat proceeds past the second sill in Boknafjorden (at km 55). Counter to canonical marine ice sheet instability theory (Weertman, 1974), retreat does not accelerate over the retrograde slope around km 55–65. This part of the bed coincides with the narrow entrance (bottleneck) to the inland Nedstrandsfjorden (Fig. 4). Retreat and flow accelerate again at the end of the overdeepened bed (at km 70) and up the prograde bed towards km 80. Here, the glacier stabilises with a steep surface just upstream of the grounding line. The steady-state velocities close to the front vary by a factor of three over less than 10 km, in stark contrast to the dynamics of the flatter initial surface topography at 18 ka (Fig. 6).

Fig. 7a shows the 18 ka and perturbed steady-state grounding lines for experiments with our reference and perturbed melt rates, 20 and 100 m a^{-1}, respectively. There is little difference between grounding lines associated with 100 and the more extreme 200 m

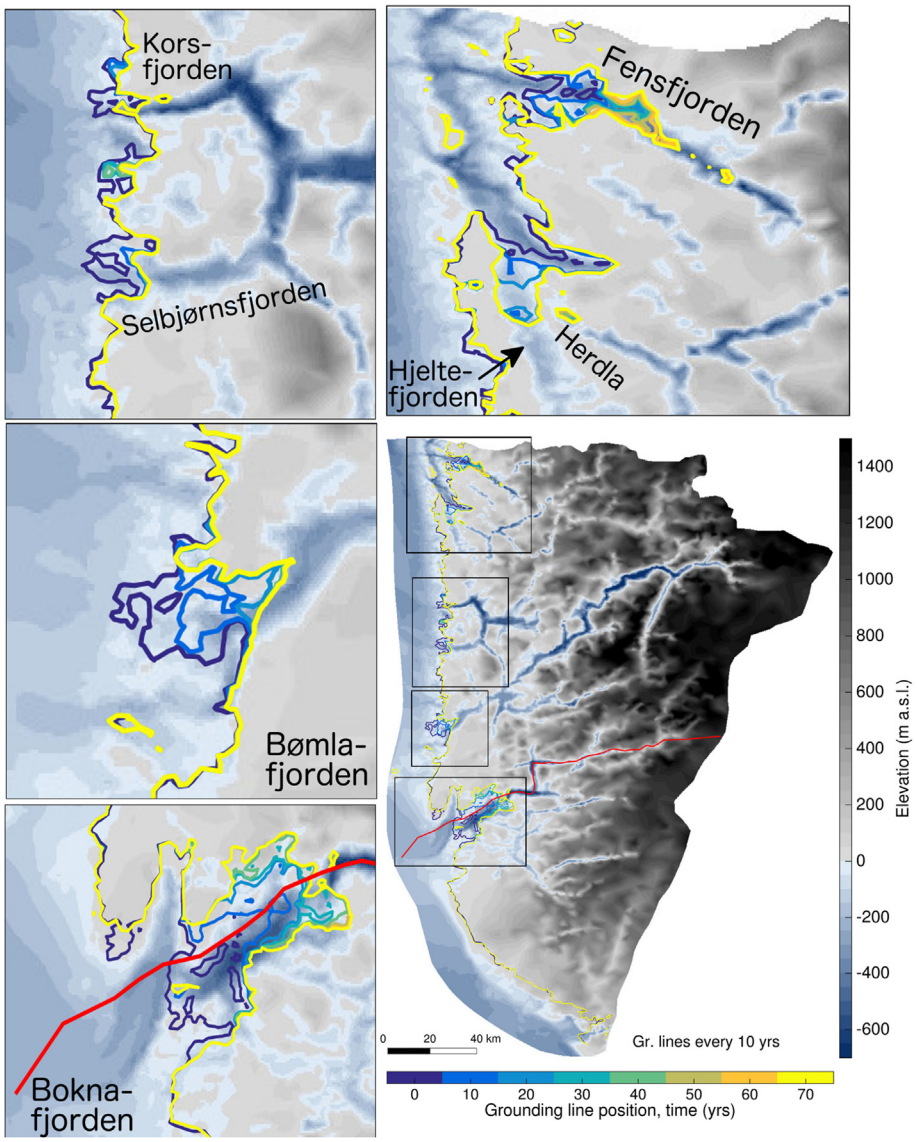

Fig. 4. Ocean forcing as a selective trigger: regional modelled grounding line positions every ten years in response to a uniform five-fold increase in submarine melt rate (from 20 to 100 m a^{-1}). For clarity, the grounding lines are only shown for the first 70 years following the perturbation (the steady state response is shown in Fig. 7a). At this time, grounding lines have stabilised in new configurations. Retreat proceeds far inland in the northern and southernmost fjords, whereas little change occurs in narrow inlets in the central parts of the west coast. The flowline for the Bokna-Vindafjorden ice stream is shown in red, with details given in Figs. 5 and 6. (For interpretation of the references to colour in this figure legend, the reader is referred to the Web version of this article.)

a^{-1} melt rate. The exception is Boknafjorden, where the grounding line is dislodged from a sill located in a lateral constriction of the fjord, and thereby migrates into the inland Nedstrandsfjorden, as shown along its flowline in Fig. 6.

5.3. Surface mass balance: a slow trigger and long-term driver

In our second set of sensitivity experiments, we raise the ELA relative to the 18 ka state, as described in Sect. 4.2. Here we describe the 300 m ELA rise. To put this forcing in perspective, the air temperature following the Younger Dryas cold reversal (See Sect. 5.4 for more details) may have increased by 4–5 °C in southern Norway (Birks et al., 2013), accompanied with ELA increases of up to 300–500 m (Lie et al., 2003b; Mangerud et al., 2013, 2016).

As with the ocean forcing, the model shows a spatially variable response to the regionally uniform ELA increase of 300 m (Fig. 7b). This imposed step increase of the ELA corresponds to an instantaneous inland migration of the ELA by c. 30–40 km, depending on the topographic setting. Retreat due to atmospheric warming and ELA rise is more extensive than the response to ocean warming and enhanced submarine melt, particularly for land-based ice. The flat Jæren area in the south and the dynamic Boknafjorden ice stream experience the most extensive retreat (Fig. 7b). Most of the margin in this region is on the verge of transitioning from marine-to land-terminating ice in response to the ELA change.

Ice in the central fjords of our domain (Bømla-Hardangerfjorden, Selbjørnsfjorden, Korsfjorden) retreat 20–25 km inland of their 18 ka margins. Retreat is more modest in the central fjords than in the nearby Bergen area to the north. This results in a complex ice sheet margin, where uplands generally become ice-free first. In contrast, marine-terminating glaciers survive, fed by upstream ice discharge and pinned by topography in an otherwise too warm climate for land-based ice to persist. Conversely, the

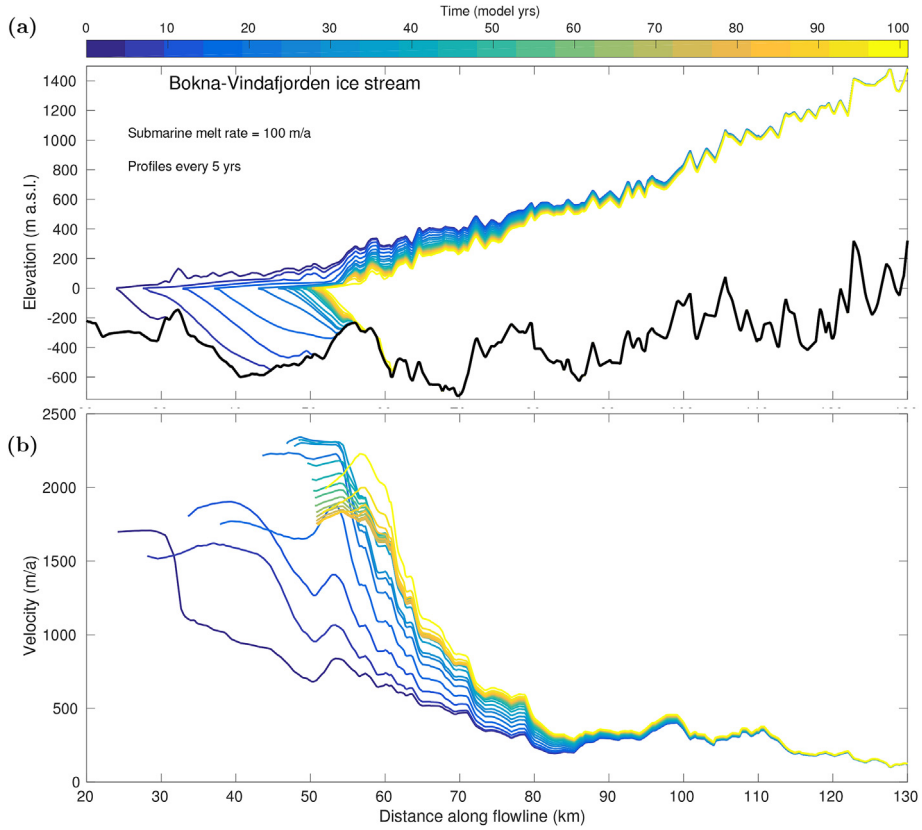

Fig. 5. Bedrock topography modulates response to ocean forcing. Glacier geometries and velocities along the flowline in Boknafjorden (Fig. 4) are shown every five years, in response to a five-fold increase in submarine melt rate, from 20 to 100 m a^{-1}.

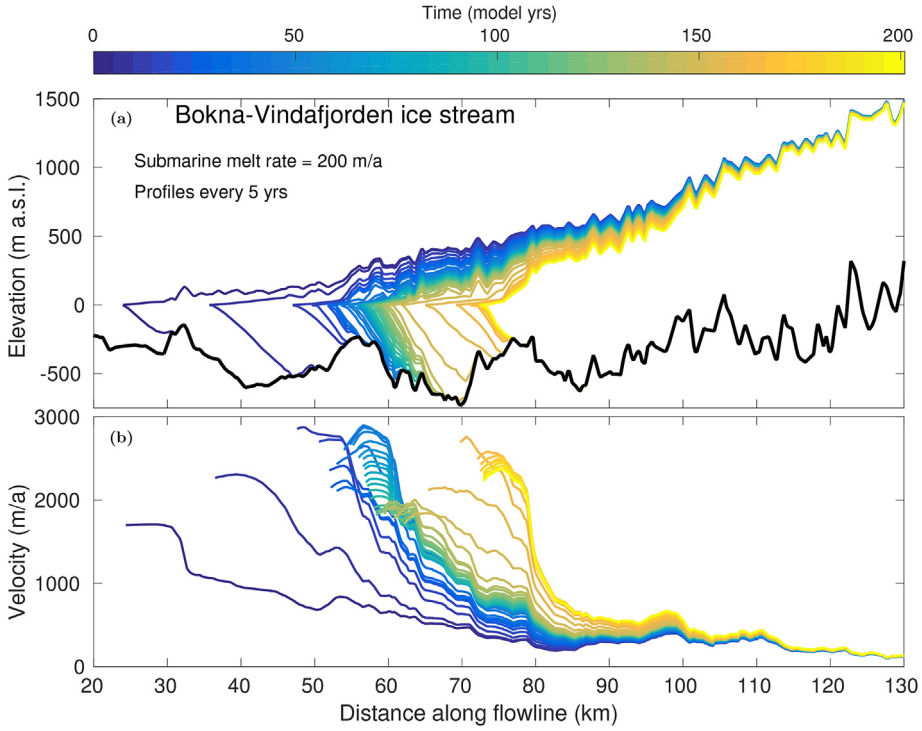

Fig. 6. Bedrock topography modulates response to ocean forcing. Glacier geometries and velocities along the flowline in Boknafjorden (Fig. 4) are shown every five years, in response to a step ten-fold increase in submarine melt rate, from 20 to 200 m a^{-1}.

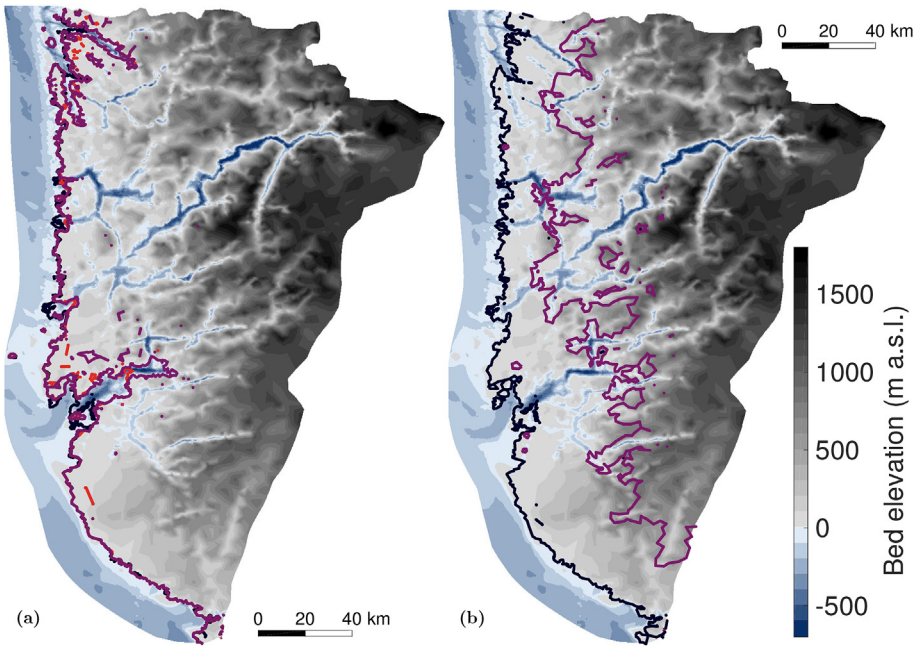

Fig. 7. Heterogeneous response to regionally uniform changes in forcing. Shown are initial (black) and perturbed steady-state grounding lines (below sea level) and ice margins (on land), for (a) an increase in submarine melt rate from 20 to 100 m a^{-1} (red) and 200 m a^{-1} (purple); and (b) an ELA rise by 300 m (purple). Note the relatively large retreat in the southern and northern fjords compared to the central areas of the west coast. (For interpretation of the references to colour in this figure legend, the reader is referred to the Web version of this article.)

marine based Boknafjorden ice stream retreats further inland than the nearby land based ice.

We find that from the 18 ka state, a warmer atmosphere with elevated ELA (Fig. 7b) causes substantially more ice volume loss than our most extreme ocean warming with 200 m a^{-1} submarine melt rates (Fig. 7a). As an example, raising the ELA by 300 m increases the surface melt and ice discharge by a factor of two.

A summary of the experiments starting from the 18 ka state employing a range of ELA and submarine melt rates is shown in Fig. 8. However, a fair comparison between magnitudes of ELA changes and submarine melt rates is not straightforward. For small changes of the ELA, more ice is retained in the fjords and a warmer ocean is indeed important. For example, a 100 m ELA increase combined with five times higher submarine melt rates yields 40% more mass loss than the ELA increase alone. Note that submarine melt rates are an order of magnitude higher than surface melt rates (cf. Sect. 3.3 and 4.2), yet submarine melt affects a significantly smaller area than does the surface melt across the ablation area. For larger ELA changes, much of the margin becomes land-terminating (Fig. 7b). Beyond this point (an ELA increase of c. 300 m), surface mass balance almost completely determines the amount of mass lost (Fig. 8).

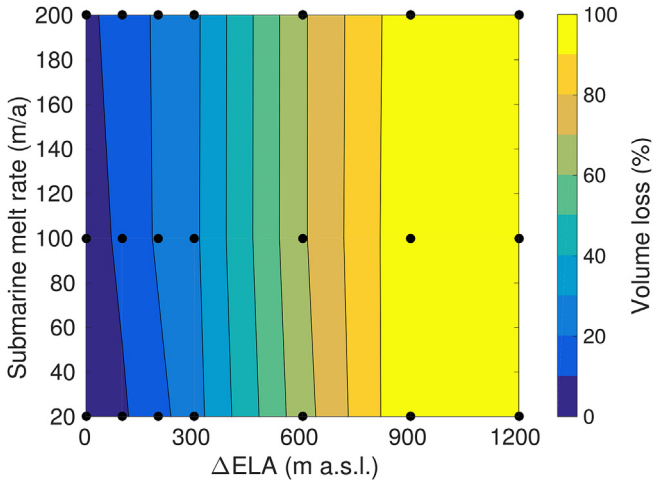

Fig. 8. Loss of volume above flotation in response to changes in submarine melt rate and ELA, with the 18 ka ice sheet as initial conditions. Black dots represent individual model experiments. For reference, the Younger Dryas and present-day ELA are estimated to be ~500 m and ~1000 m above the ELA at 18 ka, respectively (Lie et al., 2003a; b; Andreassen et al., 2012; Mangerud et al., 2016).

5.4. Simulated deglaciation of western Norway

In the previous sections, the sensitivity experiments employ constant perturbations starting from a fixed 18 ka climate. In contrast, now we run the model with time-varying climate forcing approximating the deglaciation from 18 to 11 ka (Sect. 4.3), including a time-varying ELA and submarine melt (Fig. 9a). We are thus in a position to compare our model results with independent empirical evidence (Fig. 10). Note, that the submarine melt rate is scaled to the ELA, as described in Sect. 3.4 (Eq. (7)).

For the deglaciation 18–11 ka, our model results suggests that the Boknafjorden and Jæren areas to the south are the most sensitive to changes in climate. Consistent with reconstructions and our sensitivity experiments outlined in Sect. 5.2 and 5.3, this is where marine-based ice retreats first, progressing into the wide, deep trough inland of the stabilising shallow sill between the islands Bokn and Kvitsøy (Fig. 10a).

Except for the detailed reconstructed Younger Dryas margin, our spatially continuous model history makes it possible to examine the ice margin in more detail than in the reconstructions (Fig. 2; red lines in Fig. 10). The modelled ice margin for the warm Bølling-Allerød period c. 14.8–12.7 ka BP is in good agreement with reconstructions (Fig. 10b and c). An exception is the retreat of the Hardangerfjorden glacier in the Allerød, which we are not able to

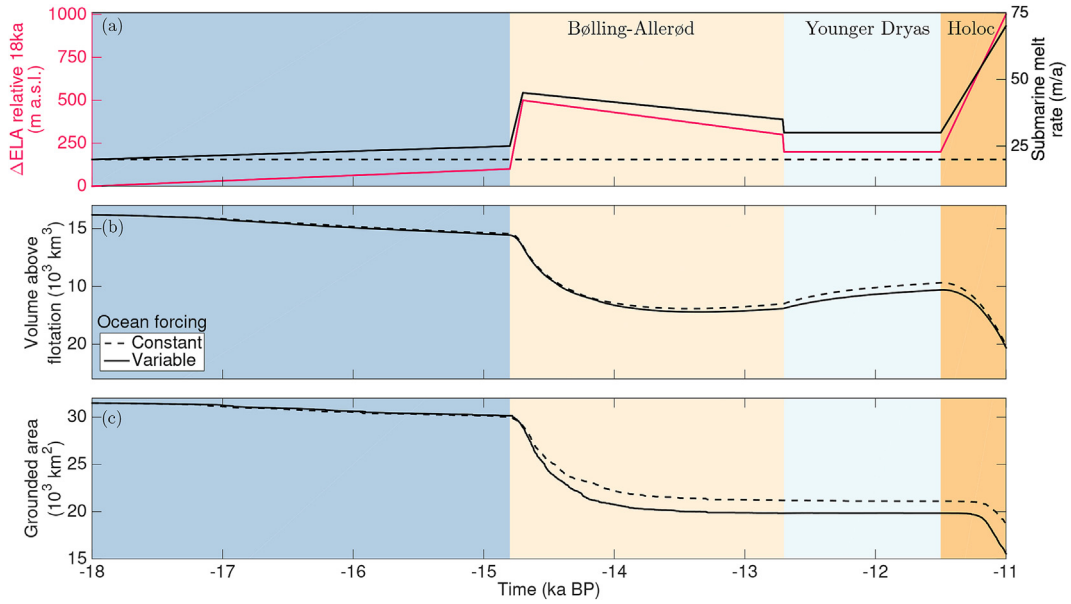

Fig. 9. Time series of (a) climate and ocean forcing (see Sect. 3.3 and 3.4 for details), (b) ice volume above flotation, and (c) grounded ice area. Volumes and areas corresponding to constant (dashed) and variable (solid) ocean forcing (submarine melt) are shown.

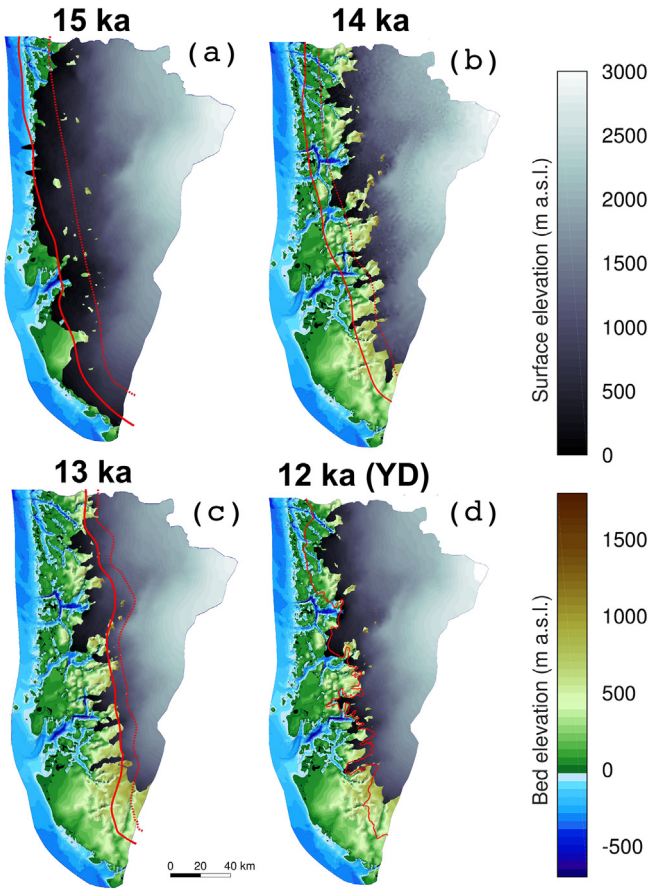

Fig. 10. Modelled ice sheet geometry at (a) 15 ka, (b) 13 ka (Allerød), and (c) 12 ka, equivalent to the Younger Dryas maximum extent. For each time-slice, red solid and dotted lines represent maximum and minimum extent from geological reconstructions (Briner et al., 2014; Hughes et al., 2016; Gump et al., 2017; Mangerud et al., 2017). (For interpretation of the references to colour in this figure legend, the reader is referred to the Web version of this article.)

capture. Retreat of this outlet glacier is also documented for the early Holocene (e.g. Mangerud et al., 2013), while the model glacier front is still located close to the Younger Dryas position (Fig. 10d) at the end of our simulation at 11 ka (not shown here). We discuss this mismatch in Sect 6.3.

Marine-based fronts generally lag retreat on land, consistent with our sensitivity experiments in Sect. 5.3. This is particularly clear during the Bølling-Allerød (Fig. 10b and c) and the Younger Dryas (Fig. 10d), resulting in an ice margin with marine-based outlet glaciers chiselled in between nearby ice-free mountains.

For the Younger Dryas cold reversal, the modelled margin is largely consistent with the reconstructions, which for this time period are highly precise. There is a small mismatch in the southern part of the model domain, likely due to the influence of the nearby domain boundary. We also underestimate the well-documented advance in the north (Mangerud et al., 2016). However, overall the agreement between the model and the reconstructions is excellent for the Younger Dryas.

We end our simulation in the early Holocene (11 ka). At this time, the model fits well with reconstructions in the south, while ice margin retreat in the north is underestimated (not shown here).

Overall, we find that temporally variable ocean forcing has a minor effect on long-term mass loss over the course of the deglaciation in south-western Norway (Fig. 9). Differences between model experiments with and without variable oceanic melt only causes a difference of 4% in mass loss during the Younger Dryas (Fig. 9b).

6. Discussion

6.1. Atmospheric warming drives deglaciation

Our sensitivity experiments and 18–11 ka BP simulations suggest that the deglaciation of western Norway was mainly driven by atmospheric warming, with little long-term influence by the ocean. The subdued importance of the ocean can be explained by a combination of small long-term upstream effects of submarine melt, and marine-based fronts becoming land-terminating. In addition, increased surface ablation leads to surface thinning and thereby

less ice supplied to marine-terminating fronts. Since grounding line stability depends on the upstream flux to the grounding line, and the water depth at the grounding line (e.g. Schoof, 2007), enhanced surface ablation causes 'grounding line starvation' and further retreat up the fjords.

Ocean-induced melt affects only a fraction of the area that is affected by surface melt, as mentioned in Sect. 5.3. Sustained ice sheet retreat must have required large, persistent changes in surface mass balance. This is supported by models and reconstructions of the Laurentide Ice Sheet, where surface melt rather than dynamic discharge has been suggested to control ice stream activity and ice sheet mass balance (Carlson et al., 2009; Ullman et al., 2015; Stokes et al., 2016). However, this comparison is complicated by the different topographic settings, since Laurentide ice streams were active over more subdued topography than the fjord landscape of western Norway. Western Norway is more comparable to the fjord landscapes of Greenland and the Antarctic Peninsula.

In Greenland, recent dynamic retreat and acceleration is thought to have been triggered at the ice-ocean boundary (Holland et al., 2008; Murray et al., 2010), in addition to coupling between increased surface ablation and more vigorous submarine melt (Straneo and Heimbach, 2013). Similarly, ocean warming may have triggered initial retreat in the early-to middle part of the deglaciation in western Norway. For example, foraminifera-based marine reconstructions suggest up to 6 °C change in SSTs in the Norwegian Sea entering the Bølling-Allerød warm period (Eldevik et al., 2014; Dokken et al., 2015). At this time, both our model simulations and ice marginal reconstructions suggest a widespread retreat.

Our simulated ocean-triggered retreat and resulting initial dynamic surface thinning in western Norway support the hypothesis that recent observed retreat of marine-terminating glaciers in Greenland was triggered by the ocean. Further, our results are consistent with the inference that the ocean will continue to exert control on Greenland marginal mass loss over the next few decades. However, based on our experiments, we expect that widespread retreat and substantial deglaciation of Greenland on time scales beyond a few decades will be driven primarily by atmospheric warming and surface melt.

In reality, higher surface melt leads to increased runoff, subglacial discharge and increased buoyancy driven oceanic melt at the ice-ocean interface (Slater et al., 2016). As a consequence, surface mass balance is likely to dominate on long timescales, as it also paces the mass loss at the ocean boundary. This is not explicitly resolved in our model: instead, it is implicitly accounted for by scaling the submarine melt to changes in the ELA (cf. Sect. 3.4).

Over the course of deglaciation, calculation of individual ice sheet-wide fluxes shows that rates of mass loss from surface and submarine melt are comparable in magnitude during the warm periods (Bølling-Allerød and Holocene), while ice discharge provides the largest contribution to the total rate of ice sheet mass loss (not shown here). The results also show that the submarine melt dominates over surface melt in the cold periods with extended marine terminating margins (early deglacial and Younger Dryas), with surface melt increasing in the Holocene, as the ice sheet margins retreat. Eventually, surface melt overcomes submarine melt as the ice becomes land terminating.

This behaviour is expected, as submarine melt rate in the model is scaled to the ELA forcing (cf. Eq. (7)). In other words, given no change in the floating area, mass loss from submarine melt scales directly with the imposed ELA changes (surface melt). However, the floating area of ice is not fixed: it changes as a function of grounding line dynamics and buttressing. As a consequence, the mass loss from submarine melt is highly dependent on the total are of floating ice (cf. Fig. 9b). Given that grounding line dynamics and buttressing depend on topographic changes along the fjords (including deepening/shoaling of the bed, widening/narrowing of the trough walls), the fjord topography strongly influences the magnitude of mass loss from submarine melt.

In a warming climate, sea-level rise may act as a positive feedback for glaciers close to flotation, rendering glaciers terminating in deeper water vulnerable, potentially causing more vigorous calving and retreat (e.g. Brown et al., 1982; Warren, 1992). This argument can be ruled out for the deglaciation of the western Scandinavian Ice Sheet, since relative sea level was falling along the coast of western Norway (Lohne et al., 2007; Lunnan, 2016).

We find that the Boknafjorden ice stream and the flat Jæren area was the most sensitive sector in western Norway, consistent with reconstructions of early deglaciation in this region. The deep, wide trough in Boknafjorden makes it particularly vulnerable to unstable grounding line retreat (e.g. Schoof, 2007; Jamieson et al., 2012; Åkesson et al., 2018), while the low-lying Jæren region is deprived from the supply of upstream ice in our simulations, making it highly sensitive to increased surface melt. Our results suggest that the fjords act to channel ice from upstream accumulation areas towards otherwise ice-free coastal regions. Upstream ice discharge is the main control of long-term retreat, rather than retreat being dominated by warm ocean water at the terminus. An efficient resupply of ice is not possible for Jæren, since this region is not fed by any fjords or upstream valleys, and is ~70–90 km away from large accumulation areas located in the vast interior mountain plateau. In the central and northern parts of western Norway, this mountain plateau extends closer to the coast (Mangerud et al., 2011, p. 291) and transitions into deep valleys and fjords over distances of ~5–30 km (Fig. 2).

To summarise, with increased surface melt, our simulations suggest that high mountain areas along the coast become ice-free first, while marine-terminating glaciers in fjords tend to survive. This pattern is consistent with contemporary changes in Greenland, where outlet glaciers in fjords persist even when exposed to extensive melt because they are efficiently fed by large accumulation areas upstream. In contrast, dynamically stagnant ice on uplands are more vulnerable to surface melt.

6.2. Retreat and readvance modulated by topography

The model simulations exhibit an excellent fit with the reconstructed marginal positions for the Younger Dryas (Fig. 10d). This agreement is rather remarkable considering our simplified representation of surface mass balance, ice dynamics, ocean forcing and temporally invariant basal friction. Despite these simplifications, the model is close to the empirically well-documented ice sheet margin. We therefore suggest that the role of subglacial hydrology and ice-ocean interactions are not critical in providing a first-order picture of long-term ice sheet evolution and sensitivity. We also note that the modelled ice sheet margin at this time is largely land-based, incised by a few marine-terminating glaciers in deep fjords.

Ample evidence support the YD as a major climatic event involving both the atmosphere and the ocean (e.g. Bakke et al., 2009; Eldevik et al., 2014), and that the large-scale readvance during the YD in western Norway was driven by a change in climate. Nevertheless, the excellent fit to the reconstructed YD margin, given the many limitations of our model and forcing, leads us to hypothesise that the YD margin positions were strongly modulated by the local topography.

In addition to the YD, our simulations suggest that movements of the ice sheet margin in western Norway were heavily influenced by geometry also between 18 ka and the Bølling period commencing 14.8 ka BP. Strong topographic controls of ice stream and outlet glacier retreat have been found elsewhere, including in Greenland (Hogan et al., 2016), Scandinavia (Mangerud, 1980;

Mangerud et al., 2016), Antarctic Peninsula (Jamieson et al., 2012, 2014), Patagonia (Warren, 1994), and Alaska (Mercer, 1961), though none of these include a high-resolution model of grounding line dynamics allowing for comparison across glaciers along the ice sheet margin.

Because of their strong dependency on topography, individual marine-terminating glaciers are questionable climate indicators (Mann, 1986; Post et al., 2011). Our asynchronous, simulated retreat during deglaciation in western Norway supports this idea, and is also consistent with the highly variable observed retreat for Greenland outlet glaciers (e.g. Moon and Joughin, 2008; Hill et al., 2017). In Greenland, fjord geometry has been suggested as key to both the stability of glacier fronts (Morlighem et al., 2016), and the sensitivity to submarine melt, surface melt and subglacial discharge (Bartholomaus et al., 2016; Motyka et al., 2017), as well as the extent of upstream thinning following terminus retreat (Felikson et al., 2017). Studying the detailed impact of each of these factors on paleo-time scales remains a focus for future work.

Our findings, and the growing amount of evidence for Greenland's outlet glaciers, suggest that present-day changes to glaciers include geometric influences that may be overlooked, or worse, falsely attributed to external forcing. This reasoning does not contradict marine-terminating glaciers as vulnerable to a warming climate, but individual glacier behaviour is not a sufficient basis to infer regional patterns. Given that stable positions are largely determined by the underlying topography, we may also turn the problem around and seek to estimate stable (moraine) positions in the past and future by studying the (three-dimensional) bedrock topography.

To the authors' knowledge, this is the first study to finely resolve the deglaciation of multiple fjords over a large coastal region. The experiments presented here are focused on south-west Norway, but are important for our understanding of other regions with past or present marine-terminating glaciers, including Greenland, Alaska, Patagonia, Svalbard, and the Antarctic Peninsula. Our simulations demonstrate a new avenue for high-resolution, continuous paleoclimate model studies at spatial scales approaching those for which geological evidence is collected.

6.3. Model limitations

We use the Shelfy Stream Approximation (SSA) to simulate ice flow. This approximation neglects vertical shear and is therefore suitable in areas of fast flow, such as marine-terminating glaciers and ice shelves. However, SSA is less accurate in the interior of ice sheets where vertical shear dominates. Thus, we expect that our model underestimates flow from the interior, giving a slightly too thick ice near the ice divide. However, 2D SSA has been shown to capture ice flow even in regimes where its applicability should be limited (Larour et al., 2012). In addition, we expect that uncertainty in the surface mass balance will be more important than differences due to approximations in the representation of ice flow.

Neither in the Allerød period (Fig. 10c), nor in the early Holocene (not shown) are we able to capture the documented retreat of the Hardangerfjorden glacier. This may be because we do not include calving in our model, as explained in Sect. 3.1. Including a calving law is therefore a priority for future work.

In the north of the domain, we underestimate the ice sheet retreat following the Younger Dryas. At this time, the margins in this region are mostly land-based. This suggests that we may underestimate surface ablation, or that the simulated Younger Dryas ice sheet is too thick and therefore able to persist during the early Holocene.

Glacial isostatic adjustment (GIA) is not included in our simulations. Shoreline diagrams indicate a postglacial emergence of ~100 m in the inner Hardangerfjorden area (Mangerud et al., 2016), decreasing towards the coast. This may lead to the model overestimating the surface elevation of ice, in particular for the interior. However, uplift has been minor along the coast due to the smaller ice load. Therefore, we expect that our exclusion of GIA has little impact on our modelled grounding line dynamics.

We do not model sediment dynamics, hydrology or thermal regime explicitly, due to their unconstrained nature, and to keep computational needs down. However, we expect that temperate basal conditions prevailed in the fjords throughout the deglaciation. This is supported by numerous glacial striae, p-forms and ice-front deposits consisting of glaciofluvial sediments (e.g. Hamborg and Mangerud, 1981; Sollid and Sørbel, 1994; Mangerud et al., 2011; Sæle, 2017). Sediment cover is sparse at present, and we do not expect that sediment thickness varied considerably during deglaciation. However, we acknowledge that our parameterization of basal motion (Sect. 3.2) is simple, and future experimental work will elaborate on the effects of different parameterizations. Our results also suggest that the details of these processes may not be required when estimating ice sheet sensitivity to a first-order (see Sect. 6.2).

Regarding the ocean forcing, we refrain from adding additional parameters and keep submarine melt rates depth-independent. Observations and models suggest that melt rates vary with depth with a maximum at a given depth above the grounding line (Jenkins, 2011). In addition, undercutting by warm fjord water may influence calving rates (O'Leary and Christoffersen, 2013; Rignot et al., 2015; Benn et al., 2017). As we exclude calving dynamics in our simulations, we may somewhat underestimate the sensitivity of the model to the ocean forcing. However, we do not expect this to change our main conclusions.

While we do not include explicit calving in the model, submarine melt is applied to the floating ice and modulates the length and thickness of any floating tongues present. In this respect, the imposed ocean forcing implicitly acts as a variable calving rate. The ocean forcing also affects the upstream ice by changing the buttressing of the floating tongue. This has been shown to stabilise grounding lines located in otherwise 'unstable' topographic settings, such as retrograde (upstream deepening) beds and widening troughs (Gudmundsson et al., 2012; Gudmundsson, 2013; Schoof et al., 2017; Åkesson et al., 2018). We expect that the additional buttressing associated with the neglected explicit calving renders a slightly delayed and subdued response of marine-terminating parts of the ice sheet margin in our model. We note that for grounded termini, without floating tongues, the submarine melt applied in the model would have no impact. This is not strictly consistent with observations of grounded marine-terminating glaciers in Greenland.

6.4. Implications for past and future ice sheet stability

Our experiments emphasise that warm ocean water is a *selective* trigger for glacier retreat, and that basal sills and fjord constrictions may delay or even prevent continued retreat. However, once triggered, retreat and thinning may be rapid, since geometric features lead to glaciers responding out-of-sync with their external forcing, as manifested by retreat rates higher than 800 m a^{-1} for the Boknafjorden ice stream in our sensitivity experiments (Fig. 5). Such short-lived behaviour will likely be missed and interpretations biased accordingly in low-resolution geological evidence, or worse, if evidence is overridden and destroyed by an advancing ice sheet. This highlights the advantages of using a detailed numerical ice sheet model together with geological data to study long-term changes.

The behaviour found in our study corroborates recent

observations of accelerated yet spatially variable Greenland outlet glacier retreat over the last two decades (Moon and Joughin, 2008; Howat and Eddy, 2011; Straneo and Heimbach, 2013). However, fast retreat is not likely to be sustained in the long-term, as illustrated by our modelled slowdown and stabilisation of the Boknafjorden ice stream at a new basal pinning point after 30–40 years (Fig. 5). Similarly, decadal-scale stabilisation on basal pinning points has been found in ocean-forced experiments focusing on the sensitivity of Greenland outlet glaciers to future warming (Morlighem et al., 2016; Choi et al., 2017).

Our results suggest that the ocean is a potential trigger for glacier retreat, and can dominate decadal-scale mass loss. However, for large-scale retreat over multiple centuries to millennia the surface mass balance dominates. In other words, ice-ocean interactions and grounding line dynamics can control the short-term response of outlet glaciers, while surface mass balance controls the long-term ice sheet response. This result has important implications for the future of the Greenland and East Antarctic Ice Sheets, as well as for paleo-ice sheets. These ice sheets will, to a varying extent, all transition from marine-to land-terminating ice sheets, similar to our modelled history of the deglaciation of the western Scandinavian Ice Sheet. Note, that for regions with widespread marine-terminating margins, the ocean has a strong influence. For example, during times in the past when the Greenland Ice Sheet extended to the continental shelf, we expect ice-ocean interactions to have been the major drivers of ice sheet retreat. Similarly, West Antarctica rests on a marine-based bed extending far inland (Fretwell et al., 2013), and is expected to be vulnerable to warming ocean conditions for a significantly longer period of time (Hillenbrand et al., 2017).

7. Conclusion

We have used a high resolution two-dimensional ice sheet model with detailed grounding line dynamics and simplified physics and climatology to study deglaciation of the western Scandinavian Ice Sheet, and its sensitivity to ocean and atmosphere forcing.

Our experiments suggest that the ocean is a potent yet selective trigger of decadal scale grounding line retreat for the marine-terminating margins of the ice sheet covering western Norway. In contrast, we find that longer term mass loss over the course of the deglaciation of western Norway was dominated by surface melt, with the ocean playing a minor role. Once a retreat is triggered, the simulated extent and rate of retreat is highly dependent on the presence of sills and lateral constrictions in the fjords.

In south-western Norway, the Boknafjorden ice stream and the Jæren area to the south are the most sensitive to climate change. Boknafjorden's deep, wide trough makes it geometrically unstable and more vulnerable to warm subsurface waters, resulting in a transient rapid grounding line retreat of up to 800 m a^{-1}. The flat Jæren area lacks upstream supply of ice, and is therefore highly sensitive to increased surface melt.

The details of our modelled ice sheet margins are heavily influenced by topography. This is particularly important for the widespread readvance during the Younger Dryas cold-reversal c. 12.7–11.6 ka BP. We reproduce the reconstructed Younger Dryas margin with excellent detail, despite our simple forcing and model physics. When estimating first-order ice sheet sensitivity, we therefore suggest that the details of basal motion and ice-ocean interactions are not critical, and that individual outlet glaciers may respond out-of-phase with ambient climate forcing. However, high model resolution is needed to capture topographic effects and grounding line migration accurately.

Our findings imply that ice-ocean interactions and grounding line dynamics are fundamental to short-term ice sheet mass loss. These are the likely controls of decadal to centennial scale responses of outlet glaciers and require high-resolution representation in models. For long-term past and future changes on centennial to millennial scales, our experiments suggest that atmospheric changes are the main drivers of mass loss and resulting sea level rise.

Author contributions

JIS, JM, and KHN came up with the idea of the study, HÅ, KHN, and MM refined the ideas and designed the model experiments, MM provided the ice sheet model, HÅ implemented necessary model developments specific to this study together with MM, HÅ performed model simulations with significant input from MM and KHN. Model results were analysed by HÅ, MM, and KHN, with feedback from JIS and JM. HÅ wrote the paper and made all the figures, with considerable contributions from MM, KHN, and JM. JIS gave valuable feedback on the final version of the manuscript.

The authors declare that this research was conducted without any potential conflicts of interest.

Funding

The research leading to these results was funded by the Research Council of Norway (project no. 229788), as part of the project Eurasian Ice Sheet and Climate Interactions (EISCLIM) led by JIS. The Research Council of Norway also supported a research stay for HÅ at the University of California, Irvine (project no. 261582). HÅ's research stay was also partly funded by a scholarship from Meltzerfondet at the University of Bergen, and the Norwegian Research School in Climate Dynamics. The research has also received support from the European Research Council under the European Community's Seventh Framework Programme (FP7/2007–2013)/ERC grant agreement 610055 as part of the ice2ice project. We acknowledge access to computation facilities through the NOTUR project NN4659K "Models of past ice and climate", supported by the Research Council of Norway.

Acknowledgements

We wish to thank Anna Hughes, Dale Gump, and Jason Briner for assisting with local (published) reconstructions, Johannes Bondzio for help with model development, Lev Tarasov for sharing large-scale (unpublished) model output, as well as Haflidi Haflidason and Kristian Vasskog for sharing knowledge about local geology and climate history. We are also very grateful to Andreas Vileli and an anonymous reviewer for the many constructive comments received during the review process.

Appendix A. Supplementary data

Supplementary data related to this article can be found at https://doi.org/10.1016/j.quascirev.2018.07.004.

References

Aa, A., Mangerud, J., 1981. Glasialgeologi og vegetasjonsinnvandring i indre Nordhordland, Vest-Norge (English Summary: glacial geology and immigration of vegetation in eastern Nordhordland, western Norway). Norges geologiske undersøkelse 369, 33–75.

Aarseth, I., Mangerud, J., 1974. Younger Dryas end moraines between hardangerfjorden and sognefjorden, western Norway. Boreas 3, 3–22.

Åkesson, H., Nisancioglu, K.H., Nick, F.M., 2018. Impact of fjord geometry on grounding line stability. Front. Earth Sci. 6, 71. https://doi.org/10.3389/feart.2018.00071.

An, L., Rignot, E., Elieff, S., Morlighem, M., Millan, R., Mouginot, J., Holland, D.,

Holland, D., Paden, J., 2017. Bed elevation of Jakobshavn Isbræ, West Greenland, from high-resolution airborne gravity and other data. Geophys. Res. Lett. 44, 3728–3736.
Andersen, B.G., 1954. Randmorener i Sørvest-Norge. Norsk Geografisk Tidskrift 14, 273–342.
Andersen, B.G., Wangen, O.P., 1987. Quaternary geology of Jæren and adjacent areas, southwestern Norway. Norges geologiske Undersøkelser 411, 1–55.
Andreassen, L., Winsvold, S., Paul, F., Hausberg, J., 2012. Inventory of Norwegian glaciers, 38-2012. NVE Rapport, Oslo, pp. 1–242.
Andreassen, L.M., Elvehøy, H., Kjøllmoen, B., Engeset, R.V., Haakensen, N., 2005. Glacier mass-balance and length variation in Norway. Ann. Glaciol. 42, 317–325.
Anundsen, K., 1972. Glacial chronology in parts of southwestern Norway. Norges geologiske Undersøkelser 280, 1–24.
Anundsen, K., 1990. Evidence of ice movement over southwest Norway indicating an ice dome over the coastal district of west Norway. Quat. Sci. Rev. 9, 99–116.
Applegate, P.J., Kirchner, N., Stone, E.J., Keller, K., Greve, R., 2012. An assessment of key model parametric uncertainties in projections of Greenland Ice Sheet behavior. Cryosphere 6, 589–606. https://www.the-cryosphere.net/6/589/2012/.
Arnold, N., Sharp, M., 2002. Flow variability in the Scandinavian ice sheet: modelling the coupling between ice sheet flow and hydrology. Quat. Sci. Rev. 21, 485–502.
Bakke, J., Lie, Ø., Heegaard, E., Dokken, T., Haug, G.H., Birks, H.H., Dulski, P., Nilsen, T., 2009. Rapid oceanic and atmospheric changes during the Younger Dryas cold period. Nat. Geosci. 2, 202–205.
Bartholomaus, T.C., Stearns, L.A., Sutherland, D.A., Shroyer, E.L., Nash, J.D., Walker, R.T., Catania, G., Felikson, D., Carroll, D., Fried, M.J., et al., 2016. Contrasts in the response of adjacent fjords and glaciers to ice-sheet surface melt in West Greenland. Ann. Glaciol. 57, 25–38.
Benn, D.I., Åström, J., Zwinger, T., Todd, J., Nick, F.M., Cook, S., Hulton, N.R., Luckman, A., 2017. Melt-undercutting and buoyancy-driven calving from tide-water glaciers: new insights from discrete element and continuum model simulations. J. Glaciol. 240, 691–702. https://doi.org/10.1017/jog.2017.41.
Birks, H.H., Kristensen, D.K., Dokken, T.M., Andersson, C., 2013. Exploratory comparisons of quantitative temperature estimates over the last deglaciation in Norway and the Norwegian sea. In: The Nordic Seas: an Integrated Perspective. American Geophysical Union, URL, pp. 341–355. https://doi.org/10.1029/158GM21.
Borstad, C.P., Rignot, E., Mouginot, J., Schodlok, M.P., 2013. Creep deformation and buttressing capacity of damaged ice shelves: theory and application to Larsen C ice shelf. Cryosphere 7, 1931–1947. https://www.the-cryosphere.net/7/1931/2013/.
Briner, J.P., Miller, G.H., Davis, P.T., Finkel, R.C., 2005. Cosmogenic exposure dating in arctic glacial landscapes: implications for the glacial history of northeastern Baffin Island, Arctic Canada. Can. J. Earth Sci. 42, 67–84.
Briner, J.P., Svendsen, J.I., Mangerud, J., Lohne, Ø.S., Young, N.E., 2014. A 10Be chronology of south-western Scandinavian Ice Sheet history during the Late-glacial period. J. Quat. Sci. 29, 370–380.
Brown, C.S., Meier, M.F., Post, A., et al., 1982. Calving Speed of Alaska Tidewater Glaciers, with Application to Columbia Glacier. USGS Professional Paper, 1258-C, p. 13.
Budd, W., Jenssen, D., Smith, I., 1984. A three-dimensional time-dependent model of the West Antarctic ice sheet. Ann. Glaciol. 5, 29–36.
Carlson, A.E., Anslow, F.S., Obbink, E.A., LeGrande, A.N., Ullman, D.J., Licciardi, J.M., 2009. Surface-melt driven Laurentide ice sheet retreat during the early Holocene. Geophys. Res. Lett. 36. https://doi.org/10.1029/2009GL040948.
Choi, Y., Morlighem, M., Rignot, E., Mouginot, J., Wood, M., 2017. Modeling the response of nioghalvfjerdsfjorden and zachariae isstrøm glaciers, Greenland, to ocean forcing over the next century. Geophys. Res. Lett. 44.
Cuffey, K.M., Paterson, W.S.B., 2010. The Physics of Glaciers. Elsevier, p. 704.
Dokken, T., Andersson, C., Risebrobakken, B., 2015. Relative abundance of planktic foraminifera and calculated SSTs and SST anomaly (11.1-25.5 ka BP) in sediment core MD95-2010f. https://doi.org/10.1594/PANGAEA.841922.
Durand, G., Gagliardini, O., Favier, L., Zwinger, T., le Meur, E., 2011. Impact of bedrock description on modeling ice sheet dynamics. Geophys. Res. Lett. 38. https://doi.org/10.1029/2011GL048892.
Dutton, A., Carlson, A.E., Long, A.J., Milne, G.A., Clark, P.U., DeConto, R., Horton, B.P., Rahmstorf, S., Raymo, M.E., 2015. Sea-level rise due to polar ice-sheet mass loss during past warm periods. Science 349. https://doi.org/10.1126/science.aaa4019.
Ehlers, J., Ehlers, J., Gibbard, P.L., Hughes, P.D., 2011. Quaternary Glaciations-extent and Chronology: a Closer Look. Elsevier, p. 1126.
Eldevik, T., Risebrobakken, B., Bjune, A.E., Andersson, C., Birks, H.J.B., Dokken, T.M., Drange, H., Glessmer, M.S., Li, C., Nilsen, J.E.Ø., et al., 2014. A brief history of climate—the northern seas from the Last Glacial Maximum to global warming. Quat. Sci. Rev. 106, 225–246.
Enderlin, E., Howat, I., Vieli, A., 2013. High sensitivity of tidewater outlet glacier dynamics to shape. Cryosphere 7, 1007–1015.
Feldmann, J., Levermann, A., 2015. Collapse of the west antarctic ice sheet after local destabilization of the amundsen basin. Proc. Natl. Acad. Sci. Unit. States Am. 112, 14191–14196.
Felikson, D., Bartholomaus, T.C., Catania, G.A., Korsgaard, N.J., Kjær, K.H., Morlighem, M., Noël, B., van den Broeke, M., Stearns, L.A., Shroyer, E.L., et al., 2017. Inland thinning on the Greenland ice sheet controlled by outlet glacier geometry. Nat. Geosci. 10, 366–369.
Follestad, B.A., 1972. The deglaciation of the south-western part of the Folgefonn peninsula, Hordaland. Norges geologiske Undersøkelser 280, 31–64.
Fretwell, P., Pritchard, H.D., Vaughan, D.G., Bamber, J.L., Barrand, N.E., Bell, R., Bianchi, C., Bingham, R.G., Blankenship, D.D., Casassa, G., Catania, G., Callens, D., Conway, H., Cook, A.J., Corr, H.F.J., Damaske, D., Damm, V., Ferraccioli, F., Forsberg, R., Fujita, S., Gim, Y., Gogineni, P., Griggs, J.A., Hindmarsh, R.C.A., Holmlund, P., Holt, J.W., Jacobel, R.W., Jenkins, A., Jokat, W., Jordan, T., King, E.C., Kohler, J., Krabill, W., Riger-Kusk, M., Langley, K.A., Leitchenkov, G., Leuschen, C., Luyendyk, B.P., Matsuoka, K., Mouginot, J., Nitsche, F.O., Nogi, Y., Nost, O.A., Popov, S.V., Rignot, E., Rippin, D.M., Rivera, A., Roberts, J., Ross, N., Siegert, M.J., Smith, A.M., Steinhage, D., Studinger, M., Sun, B., Tinto, B.K., Welch, B.C., Wilson, D., Young, D.A., Xiangbin, C., Zirizzotti, A., 2013. Bedmap2: improved ice bed, surface and thickness datasets for Antarctica. Cryosphere 7, 375–393. https://doi.org/10.5194/tc-7-375-2013.
Fried, M., Catania, G., Bartholomaus, T., Duncan, D., Davis, M., Stearns, L., Nash, J., Shroyer, E., Sutherland, D., 2015. Distributed subglacial discharge drives significant submarine melt at a Greenland tidewater glacier. Geophys. Res. Lett. 42, 9328–9336.
Fürst, J.J., Durand, G., Gillet-Chaulet, F., Tavard, L., Rankl, M., Braun, M., Gagliardini, O., 2016. The safety band of Antarctic ice shelves. Nat. Clim. Change 6, 479–482.
Gagliardini, O., Brondex, J., Gillet-Chaulet, F., Tavard, L., Peyaud, V., Durand, G., 2016. Brief communication: impact of mesh resolution for MISMIP and MISMIP3d experiments using Elmer/Ice. Cryosphere 10, 307–312.
Giesen, R., Oerlemans, J., 2010. Response of the ice cap Hardangerjøkulen in southern Norway to the 20th and 21st century climates. Cryosphere 4, 191–213. https://doi.org/10.5194/tc-4-191-2010.
Golledge, N.R., Fogwill, C.J., Mackintosh, A.N., Buckley, K.M., 2012. Dynamics of the last glacial maximum Antarctic ice-sheet and its response to ocean forcing. Proc. Natl. Acad. Sci. Unit. States Am. 109, 16052–16056.
Golledge, N.R., Kowalewski, D.E., Naish, T.R., Levy, R.H., Fogwill, C.J., Gasson, E.G., 2015. The multi-millennial Antarctic commitment to future sea-level rise. Nature 526, 421–425.
Gudmundsson, G.H., 2013. Ice-shelf buttressing and the stability of marine ice sheets. Cryosphere 7, 647–655. https://www.the-cryosphere.net/7/647/2013/.
Gudmundsson, G.H., Krug, J., Durand, G., Favier, L., Gagliardini, O., 2012. The stability of grounding lines on retrograde slopes. Cryosphere 6, 1497–1505. http://www.the-cryosphere.net/6/1497/2012/.
Gump, D.J., Briner, J.P., Mangerud, J., Svendsen, J.I., 2017. Deglaciation of boknafjorden, South-western Norway. J. Quat. Sci. 32, 80–90.
Hamborg, M., Mangerud, J., 1981. En rekonstruksjon av isbevegelser under siste istid i samnanger og kvam, hordaland, vest-norge (with English summary: a reconstruction of ice movement directions during the late weichselian in samnanger and kvam, hordaland, western Norway). Norges geologiske undersøkelse 369, 77–98.
Haseloff, M., Sergienko, O.V., 2018. The effect of buttressing on grounding line dynamics. J. Glaciol. 64, 417431. https://doi.org/10.1017/jog.2018.30.
Helsen, M., Van De Wal, R., Van Den Broeke, M., Van De Berg, W., Oerlemans, J., 2012. Coupling of climate models and ice sheet models by surface mass balance gradients: application to the Greenland Ice Sheet. Cryosphere 6, 255–272.
Hill, E.A., Carr, J.R., Stokes, C.R., 2017. A review of recent changes in major marine-terminating outlet glaciers in northern Greenland. Front. Earth Sci. 4, 111.
Hillenbrand, C.-D., Smith, J.A., Hodell, D.A., Greaves, M., Poole, C.R., Kender, S., Williams, M., Andersen, T.J., Jernas, P.E., Elderfield, H., et al., 2017. West Antarctic Ice Sheet retreat driven by Holocene warm water incursions. Nature 547, 43–48.
Hock, R., 2003. Temperature index melt modelling in mountain areas. J. Hydrol. 282, 104–115.
Hock, R., 2005. Glacier melt: a review of processes and their modelling. Prog. Phys. Geogr. 29, 362–391.
Hogan, K.A., Cofaigh, C.Ó., Jennings, A.E., Dowdeswell, J.A., Hiemstra, J.F., 2016. Deglaciation of a major palaeo-ice stream in disko trough, west Greenland. Quat. Sci. Rev. 147, 5–26.
Holland, D.M., Thomas, R.H., De Young, B., Ribergaard, M.H., Lyberth, B., 2008. Acceleration of Jakobshavn Isbrae triggered by warm subsurface ocean waters. Nat. Geosci. 1, 659–664.
Holtedahl, H., 1975. The geology of the Hardangerfjord, west Norway. Norges geologiske Undersøkelser 322, 1–87.
Howat, I.M., Eddy, A., 2011. Multi-decadal retreat of Greenland's marine-terminating glaciers. J. Glaciol. 57, 389–396.
Hubbard, A., Bradwell, T., Golledge, N., Hall, A., Patton, H., Sugden, D., Cooper, R., Stoker, M., 2009. Dynamic cycles, ice streams and their impact on the extent, chronology and deglaciation of the British–Irish ice sheet. Quat. Sci. Rev. 28, 758–776.
Hughes, A.L., Gyllencreutz, R., Lohne, Ø.S., Mangerud, J., Svendsen, J.I., 2016. The last Eurasian ice sheets–a chronological database and time-slice reconstruction, DATED-1. Boreas 45, 1–45.
Huss, M., Farinotti, D., 2012. Distributed ice thickness and volume of all glaciers around the globe. J. Geophys. Res.: Earth Surface 117. https://doi.org/10.1029/2012JF002523. F04010.
Hutter, K., 1983. Theoretical Glaciology: Material Science of Ice and the Mechanics of Glaciers and Ice Sheets. Reidel.
Jamieson, S.S., Vieli, A., Cofaigh, C.Ó., Stokes, C.R., Livingstone, S.J., Hillenbrand, C.-D., 2014. Understanding controls on rapid ice-stream retreat during the last

deglaciation of Marguerite Bay, Antarctica, using a numerical model. J. Geophys. Res.: Earth Surface 119, 247–263.
Jamieson, S.S., Vieli, A., Livingstone, S.J., Cofaigh, C.Ó., Stokes, C., Hillenbrand, C.-D., Dowdeswell, J.A., 2012. Ice-stream stability on a reverse bed slope. Nat. Geosci. 5, 799–802.
Jenkins, A., 2011. Convection-driven melting near the grounding lines of ice shelves and tidewater glaciers. J. Phys. Oceanogr. 41, 2279–2294.
Johnsen, I., 2017. Strandforskyvning På Bokn Og Deglasiasjonen Av Boknafjorden, Rogaland [unpublished]. Master's thesis University of Bergen.
Joughin, I., Smith, B., Shean, D., Floricioiu, D., 2014. Brief communication: further summer speedup of Jakobshavn Isbræ. Cryosphere 8, 209–214.
Kleman, J., Fastook, J., Stroeven, A.P., 2002. Geologically and geomorphologically constrained numerical model of Laurentide Ice Sheet inception and build-up. Quat. Int. 95, 87–98.
Kleman, J., Hättestrand, C., 1999. Frozen-bed fennoscandian and Laurentide ice sheets during the last glacial maximum. Nature 402, 63–66.
Larour, E., Seroussi, H., Morlighem, M., Rignot, E., 2012. Continental scale, high order, high spatial resolution, ice sheet modeling using the Ice Sheet System Model (ISSM). J. Geophys. Res.: Earth Surface (2003–2012) 117 doi:0.1029/2011JF002140.
Lea, J.M., Mair, D.F., Nick, F.M., Rea, B., Weidick, A., Kjær, K.H., Morlighem, M., Van As, D., Schofield, J.E., 2014. Terminus-driven retreat of a major southwest Greenland tidewater glacier during the early 19th century: insights from glacier reconstructions and numerical modelling. J. Glaciol. 60, 333–344.
Lie, Ø., Dahl, S.O., Nesje, A., 2003a. A theoretical approach to glacier equilibrium-line altitudes using meteorological data and glacier mass-balance records from southern Norway. Holocene 13, 365–372.
Lie, Ø., Dahl, S.O., Nesje, A., 2003b. Theoretical equilibrium-line altitudes and glacier buildup sensitivity in southern Norway based on meteorological data in a geographical information system. Holocene 13, 373–380.
Lohne, Ø.S., Bondevik, S., Mangerud, J., Svendsen, J.I., 2007. Sea-level fluctuations imply that the Younger Dryas ice-sheet expansion in western Norway commenced during the Allerød. Quat. Sci. Rev. 26, 2128–2151.
Lunnan, E.M., 2016. Strandforskyvning og isavsmeltingshistorie på sørlige Karmøy. Master's thesis Universitetet i Bergen.
MacAyeal, D.R., 1989. Large-scale ice flow over a viscous basal sediment: theory and application to ice stream B, Antarctica. J. Geophys. Res.: Solid Earth (1978–2012) 94, 4071–4087.
Mangerud, J., 1980. Ice-front Variations of Different Parts of the Scandinavian Ice Sheet, 13,000-10,000 Years BP. Studies in the Lateglacial of North-West Europe, pp. 23–30.
Mangerud, J., Aarseth, I., Hughes, A.L., Lohne, Ø.S., Skår, K., Sønstegaard, E., Svendsen, J.I., 2016. A major re-growth of the scandinavian ice sheet in western Norway during allerød-younger Dryas. Quat. Sci. Rev. 132, 175–205.
Mangerud, J., Briner, J.P., Goslar, T., Svendsen, J.I., 2017. The Bølling-age Blomvåg Beds, western Norway: implications for the Older Dryas glacial re-advance and the age of the deglaciation. Boreas 46, 162–184.
Mangerud, J., Goehring, B.M., Lohne, Ø.S., Svendsen, J.I., Gyllencreutz, R., 2013. Collapse of marine-based outlet glaciers from the scandinavian ice sheet. Quat. Sci. Rev. 67, 8–16.
Mangerud, J., Gyllencreutz, R., Lohne, Ø., Svendsen, J.I., 2011. Glacial history of Norway. Dev. Quat. Sci. 279–298.
Mann, D.H., 1986. Reliability of a fjord glacier's fluctuations for paleoclimatic reconstructions. Quat. Res. 25, 10–24.
Marshall, S.J., Tarasov, L., Clarke, G.K., Peltier, W.R., 2000. Glaciological reconstruction of the Laurentide Ice Sheet: physical processes and modelling challenges. Can. J. Earth Sci. 37, 769–793.
Mengel, M., Levermann, A., 2014. Ice plug prevents irreversible discharge from East Antarctica. Nat. Clim. Change 4, 451–455.
Mengel, M., Levermann, A., Frieler, K., Robinson, A., Marzeion, B., Winkelmann, R., 2016. Future sea level rise constrained by observations and long-term commitment. Proc. Natl. Acad. Sci. Unit. States Am. 113, 2597–2602.
Mercer, J., 1961. The response of fjord glaciers to changes in the firn limit. J. Glaciol. 3, 850–858.
Millan, R., Rignot, E., Bernier, V., Morlighem, M., Dutrieux, P., 2017. Bathymetry of the amundsen sea embayment sector of west Antarctica from operation IceBridge gravity and other data. Geophys. Res. Lett. 44, 1360–1368.
Moon, T., Joughin, I., 2008. Changes in ice front position on Greenland's outlet glaciers from 1992 to 2007. J. Geophys. Res.: Earth Surface (2003–2012) 113.
Moon, T., Joughin, I., Smith, B., Howat, I., 2012. 21st-century evolution of Greenland outlet glacier velocities. Science 336, 576–578.
Morén, B.M., Sejrup, H.P., Hjelstuen, B.O., Borge, M.V., Schäuble, C., 2017. The last deglaciation of the Norwegian channel–geomorphology, stratigraphy and radiocarbon dating. Boreas. https://doi.org/10.1111/bor.12272.
Morland, L., 1984. Thermomechanical balances of ice sheet flows. Geophys. Astrophys. Fluid Dynam. 29, 237–266. https://doi.org/10.1080/03091928408248191.
Morlighem, M., Bondzio, J., Seroussi, H., Rignot, E., Larour, E., Humbert, A., Rebuffi, S., 2016. Modeling of Store Gletscher's calving dynamics, West Greenland, in response to ocean thermal forcing. Geophys. Res. Lett. 43, 2659–2666.
Morlighem, M., Rignot, E., Mouginot, J., Seroussi, H., Larour, E., 2014. Deeply incised submarine glacial valleys beneath the Greenland ice sheet. Nat. Geosci. 418–422.
Morlighem, M., Williams, C.N., Rignot, E., An, L., Arndt, J.E., Bamber, J.L., Catania, G., Chauche, N., Dowdeswell, J.A., Dorschel, B., Fenty, I., Hogan, K., Howat, I., Hubbard, A., Jakobsson, M., Jordan, T.M., Kjeldsen, K.K., Millan, R., Mayer, L., Mouginot, J., Noel, B.P.Y., O'Cofaigh, C., Palmer, S., Rysgaard, S., Seroussi, H., Siegert, M.J., Slabon, P., Straneo, F., van den Broeke, M.R., Weinrebe, W., Wood, M., Zinglersen, K.B., 2017. BedMachine v3: complete bed topography and ocean bathymetry mapping of Greenland from multi-beam echo sounding combined with mass conservation. Geophys. Res. Lett. https://doi.org/10.1002/2017GL074954.
Motyka, R.J., Cassotto, R., Truffer, M., Kjeldsen, K.K., Van As, D., Korsgaard, N.J., Fahnestock, M., Howat, I., Langen, P.L., Mortensen, J., et al., 2017. Asynchronous behavior of outlet glaciers feeding Godthåbsfjord (Nuup Kangerlua) and the triggering of Narsap Sermia's retreat in SW Greenland. J. Glaciol. 63, 288–308.
Motyka, R.J., Truffer, M., Fahnestock, M., Mortensen, J., Rysgaard, S., Howat, I., 2011. Submarine melting of the 1985 Jakobshavn Isbræ floating tongue and the triggering of the current retreat. J. Geophys. Res.: Earth Surface 116.
Murray, T., Scharrer, K., James, T., Dye, S., Hanna, E., Booth, A., Selmes, N., Luckman, A., Hughes, A., Cook, S., et al., 2010. Ocean regulation hypothesis for glacier dynamics in southeast Greenland and implications for ice sheet mass changes. J. Geophys. Res.: Earth Surface 115.
Murray, T., Scharrer, K., Selmes, N., Booth, A., James, T., Bevan, S., Bradley, J., Cook, S., Llana, L.C., Drocourt, Y., et al., 2015. Extensive retreat of Greenland tidewater glaciers, 2000–2010. Arctic Antarct. Alpine Res. 47, 427–447.
Nick, F., Van der Veen, C., Vieli, A., Benn, D., 2010. A physically based calving model applied to marine outlet glaciers and implications for the glacier dynamics. J. Glaciol. 56, 781–794.
Nick, F.M., Vieli, A., Andersen, M.L., Joughin, I., Payne, A., Edwards, T.L., Pattyn, F., van de Wal, R.S., 2013. Future sea-level rise from Greenland's main outlet glaciers in a warming climate. Nature 497, 235–238.
Nick, F.M., Vieli, A., Howat, I.M., Joughin, I., 2009. Large-scale changes in Greenland outlet glacier dynamics triggered at the terminus. Nat. Geosci. 2, 110–114.
Nowicki, S., Bindschadler, R.A., Abe-Ouchi, A., Aschwanden, A., Bueler, E., Choi, H., Fastook, J., Granzow, G., Greve, R., Gutowski, G., et al., 2013. Insights into spatial sensitivities of ice mass response to environmental change from the SeaRISE ice sheet modeling project II: Greenland. J. Geophys. Res.: Earth Surface 118, 1025–1044.
O'Leary, M., Christoffersen, P., 2013. Calving on tidewater glaciers amplified by submarine frontal melting. Cryosphere 7, 119–128.
Østrem, G., Liestøl, O., 1964. Glasiologiske undersøkelser i Norge 1963. Norsk Geografisk Tidskrift 18, 281–340.
Paolo, F.S., Fricker, H.A., Padman, L., 2015. Volume loss from Antarctic ice shelves is accelerating. Science 348, 327–331.
Patton, H., Hubbard, A., Andreassen, K., Auriac, A., Whitehouse, P.L., Stroeven, A.P., Shackleton, C., Winsborrow, M., Heyman, J., Hall, A.M., 2017. Deglaciation of the Eurasian ice sheet complex. Quat. Sci. Rev. 169, 148–172.
Pollard, D., DeConto, R.M., Alley, R.B., 2015. Potential Antarctic Ice Sheet retreat driven by hydrofracturing and ice cliff failure. Earth Planet Sci. Lett. 412, 112–121.
Post, A., O'Neel, S., Motyka, R.J., Streveler, G., 2011. A complex relationship between calving glaciers and climate. Eos, Transactions American Geophysical Union 92, 305–306.
Pritchard, H.D., Arthern, R.J., Vaughan, D.G., Edwards, L.A., 2009. Extensive dynamic thinning on the margins of the Greenland and Antarctic ice sheets. Nature 461, 971–975.
Rea, B.R., Evans, D.J., 2007. Quantifying climate and glacier mass balance in north Norway during the Younger Dryas. Palaeogeogr. Palaeoclimatol. Palaeoecol. 246, 307–330.
Reeh, N., 1989. Parameterization of melt rate and surface temperature on the Greenland ice sheet. Polarforschung 59, 113–128.
Reyes, A.V., Carlson, A.E., Beard, B.L., Hatfield, R.G., Stoner, J.S., Winsor, K., Welke, B., Ullman, D.J., 2014. South Greenland ice-sheet collapse during marine isotope stage 11. Nature 510, 525–528.
Rignot, E., Fenty, I., Xu, Y., Cai, C., Kemp, C., 2015. Undercutting of marine-terminating glaciers in West Greenland. Geophys. Res. Lett. 42, 5909–5917.
Rignot, E., Jacobs, S., Mouginot, J., Scheuchl, B., 2013. Ice-shelf melting around Antarctica. Science 341, 266–270.
Rignot, E., Koppes, M., Velicogna, I., 2010. Rapid submarine melting of the calving faces of West Greenland glaciers. Nat. Geosci. 3, 187–191.
Ringen, E., 1963. Om drumliner og Skagerakmorene på Karmøy. Norsk Geografisk Tidskrift 19, 205–228.
Ritz, C., Edwards, T.L., Durand, G., Payne, A.J., Peyaud, V., Hindmarsh, R.C., 2015. Potential sea-level rise from Antarctic ice-sheet instability constrained by observations. Nature 528, 115–118.
Robinson, A., Calov, R., Ganopolski, A., 2010. An efficient regional energy-moisture balance model for simulation of the Greenland Ice Sheet response to climate change. Cryosphere 4, 129–144.
Robinson, A., Calov, R., Ganopolski, A., 2011. Greenland ice sheet model parameters constrained using simulations of the Eemian Interglacial. Clim. Past 7, 381–396.
Rønnevik, H.C., 1971. Kvartærgeologi på ytre del av Haugesundshalvøya. Master's thesis Department of Earth Science. University of Bergen. https://bora.uib.no/handle/1956/16978.
Sæle, T.H., 2017. Skuringsstriper Og Isbevegelse for Hordaland [MSc. Thesis, Unpublished]. Master's Thesis Department of Earth Science. University of Bergen.
Schoof, C., 2007. Ice sheet grounding line dynamics: steady states, stability, and hysteresis. J. Geophys. Res.: Earth Surface 112. https://doi.org/10.1029/2006JF000664.
Schoof, C., Davis, A.D., Popa, T.V., 2017. Boundary layer models for calving marine outlet glaciers. Cryosphere 11, 2283–2303. https://doi.org/10.5194/tc-11-2283-

2017.
Sejrup, H.P., Clark, C.D., Hjelstuen, B.O., 2016. Rapid ice sheet retreat triggered by ice stream debuttressing: evidence from the North Sea. Geology 44, 355–358.
Seroussi, H., Morlighem, M., Larour, E., Rignot, E., Khazendar, A., 2014. Hydrostatic grounding line parameterization in ice sheet models. Cryosphere 8, 2075–2087. https://doi.org/10.5194/tc-8-2075-2014.
Slater, D.A., Goldberg, D.N., Nienow, P.W., Cowton, T.R., 2016. Scalings for submarine melting at tidewater glaciers from buoyant plume theory. J. Phys. Oceanogr. 46, 1839–1855.
Sollid, J.L., Sørbel, L., 1994. Distribution of glacial landforms in southern Norway in relation to the thermal regime of the last continental ice sheet. Geogr. Ann. Phys. Geogr. 76, 25–35.
Steiger, N., Nisancioglu, K.H., Åkesson, H., de Fleurian, B., Nick, F.M., 2018. Nonlinear retreat of Jakobshavn Isbræ since the little ice age controlled by geometry. Cryosphere 12, 1–18. https://doi.org/10.5194/tc-12-1-2018.
Stokes, C., Margold, M., Clark, C., Tarasov, L., 2016. Ice stream activity scaled to ice sheet volume during Laurentide Ice Sheet deglaciation. Nature 530, 322–326.
Stokes, C.R., Corner, G.D., Winsborrow, M.C., Husum, K., Andreassen, K., 2014. Asynchronous response of marine-terminating outlet glaciers during deglaciation of the Fennoscandian Ice Sheet. Geology 42, 455–458.
Straneo, F., Heimbach, P., 2013. North Atlantic warming and the retreat of Greenland's outlet glaciers. Nature 504, 36–43.
Svendsen, J.I., Briner, J.P., Mangerud, J., Young, N.E., 2015. Early break-up of the Norwegian channel ice stream during the last glacial maximum. Quat. Sci. Rev. 107, 231–242.
Tarasov, L., Dyke, A.S., Neal, R.M., Peltier, W.R., 2012. A data-calibrated distribution of deglacial chronologies for the North American ice complex from glaciological modeling. Earth Planet Sci. Lett. 315, 30–40.
Ullman, D.J., Carlson, A.E., Anslow, F.S., LeGrande, A.N., Licciardi, J.M., 2015. Laurentide ice-sheet instability during the last deglaciation. Nat. Geosci. 8, 534–537.
Van Beusekom, A.E., O'Nell, S.R., March, R.S., Sass, L.C., Cox, L.H., 2010. Re-analysis of Alaskan benchmark glacier mass-balance data using the index method. USGS Sci. Invest. Rep. 2010–5247, 1–6.
Vieli, A., Funk, M., Blatter, H., 2001. Flow dynamics of tidewater glaciers: a numerical modelling approach. J. Glaciol. 47, 595–606.
Vieli, A., Nick, F.M., 2011. Understanding and modelling rapid dynamic changes of tidewater outlet glaciers: issues and implications. Surv. Geophys. 32, 437–458.
Vieli, A., Payne, A., 2005. Assessing the ability of numerical ice sheet models to simulate grounding line migration. J. Geophys. Res.: Earth Surface (2003–2012) 110.
Van de Wal, R., 1996. Mass-balance modelling of the Greenland ice sheet: a comparison of an energy-balance and a degree-day model. Ann. Glaciol. 23, 36–45.
Van de Wal, R., Greuell, W., van den Broeke, M.R., Reijmer, C., Oerlemans, J., 2005. Surface mass-balance observations and automatic weather station data along a transect near Kangerlussuaq, West Greenland. Ann. Glaciol. 42, 311–316.
Warren, C.R., 1992. Iceberg calving and the glacioclimatic record. Prog. Phys. Geogr. 16, 253–282.
Warren, C.R., 1994. Freshwater calving and anomalous glacier oscillations: recent behaviour of Moreno and Ameghino Glaciers, Patagonia. Holocene 4, 422–429.
Weertman, J., 1974. Stability of the junction of an ice sheet and an ice shelf. J. Glaciol. 13, 3–11.